MAGNETORHEOLOGICAL ACTUATOR WITH CONTROLLABLE PERMANENT MAGNET ARRAY

By

BLAKE NELSON WILEY

A thesis submitted in fulfillment of
the requirements for the degree of

MASTER OF SCIENCE IN MECHANICAL ENGINEERING

WASHINGTON STATE UNIVERSITY
School of Engineering and Computer Science, Vancouver

DECEMBER 2019

To the Faculty of Washington State University:

The members of the Committee appointed to examine the thesis of BLAKE NELSON WILEY find it satisfactory and recommend that it be accepted

_____

Hakan Gurocak, Ph.D., Chair

_____

Stephen A. Solovitz, Ph.D.

_____

Jong-Hoon Kim, Ph.D.

ACKNOWLEDGMENT

First, I would like to thank my advisor Dr. Hakan Gurocak. Through his support and encouragement, I have grown more confident in my engineering skills and problem-solving abilities. It has been a pleasure working with someone who is so knowledgeable and has a continuously positive outlook.

I would also like to thank machinists Kurt Janzen and Chad Swanson for their aid in the design and manufacturing phase. They went above and beyond instructing me in design for manufacturing and transitioning from a concept to functioning prototype.

My gratitude also goes to Andrew Duddy with the Stack Metallurgical Group for volunteering his time for vacuum annealing. Our lab was unexperienced with this process and he was more than generous in helping our research.

Finally, I would like to thank my parents Jon and Nicole Wiley for continually supporting me in my engineering pursuits. They have each invested heavily in my education through homeschooling and allowed me the freedom to pursue my passion for engineering. Without their encouragement I would not be where I am now.

MAGNETORHEOLOGICAL ACTUATOR WITH CONTROLLABLE PERMANENT MAGNET ARRAY

Abstract

by Blake Nelson Wiley, M.S.
Washington State University
December 2019

Chair: Hakan Gurocak

This research presents a new magnetorheological brake (MRB) that uses only permanent magnets to produce variable torque output. A new magnet array was developed that can be operated by a tiny motor allowing the device to apply torque using only 1.4 Watts of electrical power. In many applications, it is desirable to have actuators with high torque output, low volume and low input power. In recent years, this has led to extensive study of MRBs because they can provide high torque-to-volume ratios when compared to electric motors of similar size. There have been many studies to optimize volume and torque, which usually leads to designs requiring complex internal magnetic flux paths and excessive power requirement resulting in joule heating and reduced performance in long-term use. Our results show that the new brake can operate for 22 hours using a small battery while cycling through full on/off torque output. It can also apply full torque output indefinitely with no power input required to keep it on. There is no joule heating since there are no coils in the design.

TABLE OF CONTENTS Page

LIST OF TABLES

LIST OF FIGURES

CHAPTER 1

INTRODUCTION

Over the past couple of decades, there has been extensive research in the field of magnetorheological brakes (MRB). They were first developed in the 1940s [1] but have recently been gaining popularity as the need for high torque density brakes has increased. They are found in robotics, haptic interfaces, safety systems, and medical equipment. MRBs utilize the unique properties of magnetorheological fluid (MRF) to generate resistive torque. The MRF is made up of micron sized ferromagnetic particles suspended in a carrier fluid. When placed in a magnetic field, the particles form chains along flux lines enabling the fluid to rapidly alter its viscosity depending on strength of the magnetic field. When no field is present, the fluid is free flowing and has a similar viscosity as a motor oil. However, when fully activated, it has a viscosity like paste.

In past work, MRBs have been studied with the purpose of optimizing maximum torque output for the smallest overall volume. This usually results in complex or large internal geometries to route flux through the MRF or increasing coils and electrical current to generate large magnetic fields ([2], [3], [4] [5], [6], [7]). While useful in many applications, these designs rarely consider the power requirements to run the MRB and thermal effects due to coil heating. In this work, an MRB is developed to overcome these shortcomings without sacrificing overall performance.

The limiting factor in previous designs is the reliance on electromagnets to generate magnetic flux. Coils are usually selected for their robustness, simplicity, and controllability with basic electronics but they have drawbacks, most significantly, their power requirements. In these devices the strength of the magnetic field is proportional to the number of coil turns and the amount of electrical current flowing through the wire. In general, a small single coil MRB requires 200-400 turns and 0-2 amps for operation.

In larger or multi-coil designs, more turns and power are needed to generate a larger magnetic field. Equation 1 defines the relationship between power required and coil geometry

$$P = I^2R = I^2\rho\frac{L}{A} \quad (1)$$

where *P* is the power, *I* is the supply current, *R* is the coil resistance, ρ is the resistivity of the wire, *L* and *A* are the length and cross-sectional area of the wire. Furthermore, the flux density in a coil is approximated in Equation 2 as:

$$B = \mu NI \quad (2)$$

where *B* is the flux density at the center of the coil, μ is the permeability of the core, and *N* is the number of turns. To generate a higher flux density resulting in higher MRB torque, the designer has three options: optimize magnetic circuit geometry, increase current or use more coils.

1.1. Property of MR-Fluid

To find ideal brake geometry, it was necessary to generate a model of the device to calculate the expected torque output. Two models are commonly used to correlate the field dependent viscosity of the MRF and the shear generated by the fluid. The simplest being the Bingham-plastic model described as:

$$\tau = \pm\tau_y(B) + \mu\dot{\gamma} \quad (3)$$

where τ is the shear stress, $\tau_y(B)$ is the yield stress as a function of the magnetic field density *B*, μ is the viscous friction coefficient and $\dot{\gamma}$ is the fluid shear rate. One downside of the Bingham model is that it does not account for the shear thickening or thinning of the MRF.

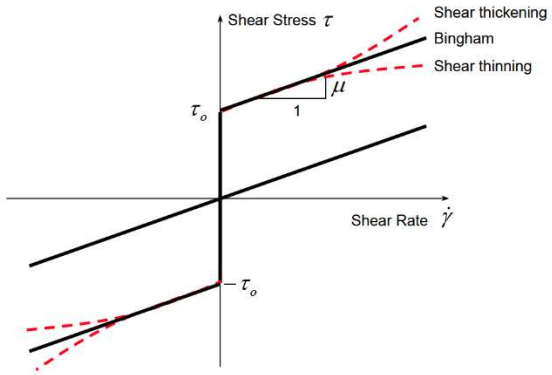

Figure 1 Typical models describing MRF shear characteristics as a function of shear rate [8]

In some MRF the fluids are not linear and behave differently at high and low shear rates. This anomaly can be accounted for by using the Herschel-Bulkley model expressed as:

$$\tau = \pm\tau_y(B) + K|\dot{\gamma}|^n \quad (4)$$

where K is the consistency factor, *n* in the flow factor. When *n*<1 the fluid is shear-thinning and n>1 is shear-thickening. It must be noted that when n=1, the equation reduces to the Bingham plastic model. At low shear rates the second term in both models is negligible and is often omitted to simplify calculations. If this simplification is used, the torque acting on a rotor can be described as:

$$dT = \tau_y(B)\, A\, dR \quad (5)$$

where *dT* is the torque, *A* is the surface area of the rotor and *dR* is the distance from the center of rotation. In most cases the fluid gap is small compared to the annular diameter so the rotor and housing are often considered parallel plates. Some studies have investigated this simplification by using an

axisymmetric model but it was found the maximum error from the parallel plate approximation is less than 5%, which is acceptable for most applications [8].

Figure 2 illustrates $\tau_y(B)$ or how the strength of a magnetic field passing through MRF effects shear yield stress for LORD Co. MRF 132DG fluid.

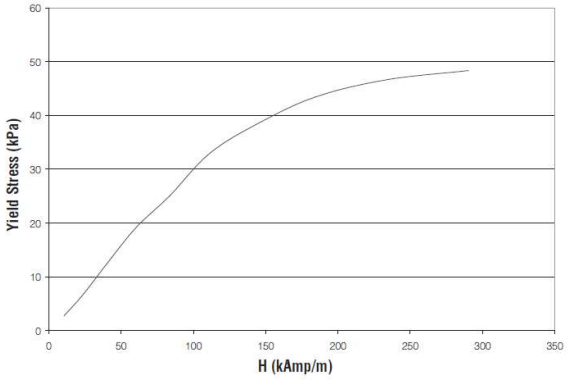

Figure 2 MRF 132 shear as a function of magnetic field strength [9]. Used in conjunction with FEA simulations to approximate MRB torque output

1.2. Related Work

MR Brakes have been designed for vastly varying applications and optimizations, but can mostly be sorted by the method each use to activate the MRF. The three types are electromagnets(EM), permanent magnet(PM) and hybrids. The following is an overview of a few brakes developed in the past six years from each category. By a large margin, most of brakes use only EMs to activate the fluid, with the second most common being the hybrid activation.

One such design is a multi-pole, double rotor MRB developed by [2]. This design used six separate coils mounted on a stator to produce a multi-pole, radial magnetic field. To efficiently utilize the geometry for maximum torque, a rotor was placed on the inner and outer surfaces of the stator. While this design

was successful in increasing the torque density, the author notes that the design has a complex structure, increasing manufacturing cost and consumes more power than comparable MRBs.

Another multi-pole design was outlined in [4]. In this paper, a multi-pole MRB is developed in an attempt to improve on single pole designs. Conventional single coil MRBs are restricted in the strength and efficiency of the magnetic field they can deliver because of geometric constraints on coil size and the need for an intricate magnetic circuit. These limitations can be avoided by using a multipole coil system which inherently causes the flux to orthogonally penetrate the fluid. A six pole stator/coil system was designed by parameterizing stator, distance between stators, and rotor ring thicknesses. Using FEA and an SNLP optimizer, dimensions were found to maximize torque and minimize total saturation at the poles. In comparison to traditional MRBs this design is simple to manufacture. It is noted that there were issues with MRF leaking, even with rubber gaskets and O-rings.

A similar multi-pole dual gap MRB was designed by [10], however they worked to minimize power consumption while maintaining torque. This design still used six radial coils mounted on a stator but implemented a bell shaped rotor rather than a dual rotor. In simulation, this design was successful in reducing the power-to-volume ratio while maintaining a similar torque density when compared to [2]. It must be noted the author did not construct a prototype to verify their findings.

Another EM based design was outlined in [6]. In this work a multi-layered drum style brake was modeled and optimized using FEA. The magnetic circuit was designed to maintain uniform flux through the fluid for varying coil currents. This results in a more linear torque to current relationship making it simpler to control. This design was optimized by varying the radii and number of fluid gaps, and fluid thickness. Each iteration was evaluated on torque density, controllability, and reactivity. The design was verified by building a physical prototype however the off state torque looks surprising low when compared to other current designs.

While not common, some research has been performed to reduce power by implementing permanent magnets(PM) in tandem with electromagnets. In these designs the idea is to use the PM as a supplementary field source to the coil and as a failsafe. The typical operation is to use the coil as a flux gate. In the OFF-torque state, the coil acts against the PM, resulting in no net flux through the MRF. In the ON state, the coil switches field directions and superimposes its flux with the PM, activating the fluid. If power is removed from the coil, the magnet is able to weakly activate the fluid on its own, creating a failsafe for the device. A device of this design has been studied by [11]. However rather than directly opposing the PM with the coil, they redirected the PM flux through a secondary magnetic circuit to prevent demagnetization. It was successful in decreasing power requirements in the ON-torque state and implementing the failsafe. The downside of this design is requiring power in the OFF-torque state to oppose the PM. Depending on duty cycle of the application, it could result in more power usage than coil-only designs.

In contrast, a coil-less MRB, utilizing a single linearly sliding PM to control the brake activation was studied by [12]. A bell shaped rotor was designed so the PM would slide easily into the cup. To control the flux reaching the fluid, a spring and pneumatic system were used to regulate the PM distance from the fluid. This resulted in a brake that could only perform in a boolean state, fully on or fully off. While no coils were required to generate activation flux, a vacuum pump and electronic valve were needed to control the sliding action of the PM, adding to the overall cost, size, and power required to run the system.

1.3. Problem Statement

In this research, a low power, continuously controllable MRB was studied that completely eliminates the use of coils for generating flux. Instead, it relies entirely on PMs. It has been shown that PM assemblies

where flux density can be mechanically altered are usually much smaller than comparable electromagnets and require no electrical power [13] making them an ideal choice for this study. Furthermore, the device was designed for simple operation, requiring minimal external components. In this way, the brake could be driven with basic electronics and a small battery for an extended length of time. As expected, the difficulty of using PMs is controlling the strength of the magnetic field. By design, they cannot be deactivated without risk of permeant demagnetization. Inspired by [11], a configuration was researched that included a secondary flux path to redirect flux rather than directly opposing the PM with another source.

CHAPTER 2

SIMPLIFIED PERMANENT MAGNET CIRCULAR HALBACH ARRAY FOR MRB

To determine the ideal permanent magnet assembly, the MRB rotor geometry first needed to be selected. The chosen geometry would dictate the MRF location and available space for permanent magnets. Figure 3 illustrates five typical and extensively studied MRB rotor geometries.

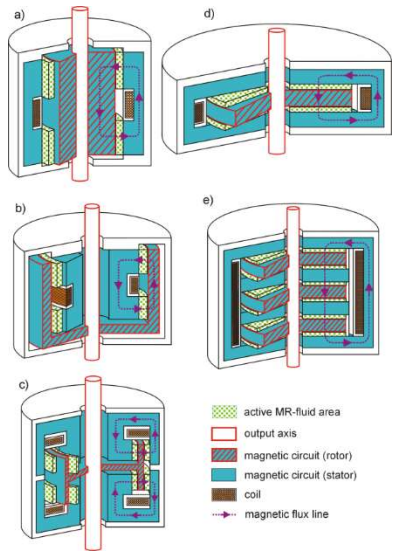

Figure 3 The five most studied MRB rotor geometries. a) drum, b) inverted drum, c) T-rotor, d) disk, e) multi-disk [14]

The suitable rotor would be space efficient and provide simple access to the magnets for mechanical activation. The two most obvious candidates are the basic drum and inverted drum. In each case, there is plenty of space for permanent magnets, however it has been shown the inverted drum can produce much higher torque than drum brakes of comparable size so it was chosen for this design. The inverted drum requires magnetic flux to travel in a radial pattern for ideal MRF activation so an adjustable permanent magnet array was needed that could fit inside the drum and generate a magnetic field perpendicular to the drum surface.

R. Bjørk published a paper comparing controllable PM assemblies to accomplish just this task [13]. They compared five different configurations and evauated each based on size and controlability. It was found the nested circular Halbach array shown in Figure 4 provided the strongest controllability, and magnetic field for the smallest volume of magnetic material. The origin of the coordinate system denotes the controllable area.

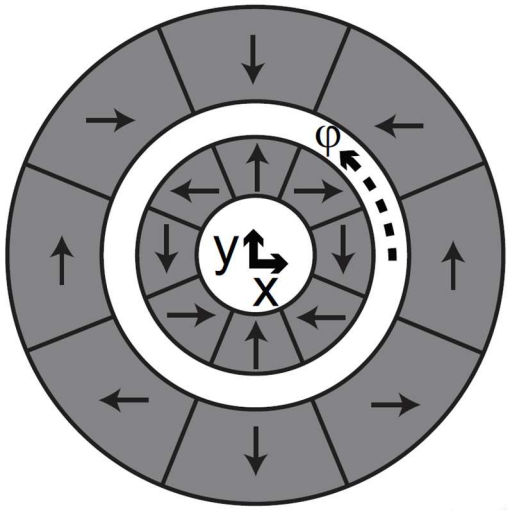

Figure 4 Nested Halbach Array consisting of arc shaped permanent magnets for controlling strength of magnetic field at the origin. The strength is continuously adjusted by rotating the two annuli by ϕ relative to each other. Figure adapted from [13]

This design would work well for a basic drum style MRB but is not ideal for use in the inverted drum configuration. Additionally, the Nested Halbach configuration is difficult and expensive to construct as the uniquely polarized arc magnets are difficult to source and the fields oppose each other during assembly.

R. Bjørk presented a simpler mangle design consisting of six individual cylinder magnets, creating a continuously adjustable array show in Figure 5.

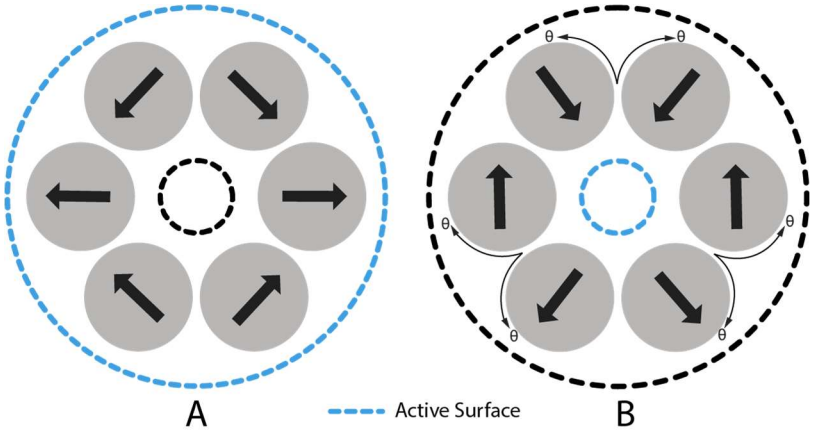

Figure 5 Mangle array consisting of six diametrically polarized cylinder magnets. In state A, the magnetic field is directed towards the outer surface shown with a blue dashed line. In state B the magnets are alternately rotated by θ, directing the magnetic field to the center

The purpose of the Six Rod Mangle array was to control the flux direction at the center, shown as the small dashed circle. To change the polarity direction, the six magnets are alternately rotated 90 degrees providing a continuously controllable field at the center. In configuration A, the flux is directed around the outer surface and in B, a strong, uniform field is generated at the center. This design would be ideal for a standard drum style rotor but an inverted drum requires the controllable region to be on the outer surface of the array, not the center.

An alternate form of a circular Halbach array is presented in [15]. The author shows two configurations for a solid annulus multi-pole Halbach array as seen in Figure 6.

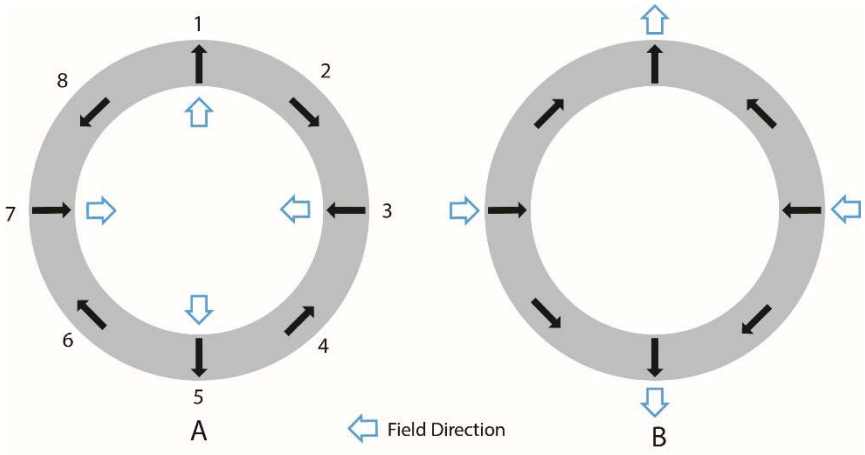

Figure 6 Solid eight section Halbach arrays in two configurations. In configuration A, the array is constructed to generate four poles on the inner surface of the array. In B, the 2,4,6, and 8 magnets are flipped 180 degrees, causing the poles to originate on the outer surface [15]

If the array is constructed in configuration A, all four poles are directed to and from the center of the annulus, resulting in almost zero residual flux on the outer surface. If it is constructed in configuration B, the polarities of magnets 2,4,6,8 are flipped 180 degrees, redirecting the poles to the outer surface. This design would be ideal for an inverted drum style brake if the poles were continuously adjustable but in this case, they are not. In an MRB application, we need to be able to vary the field continuously so that the device can produce a range of forces/torques. Fortunately, such arrays have been studied in the past, the most applicable being an adjustable linear version of the four-pole, solid Halbach array [16] shown in Figure 7. This particular array was developed as a magnetic latch. If a ferrous metal plate is placed in the high magnetic field, there is a strong pull force towards the magnets. However, as the array transitions the field to the other side, the pull force smoothly varies to zero.

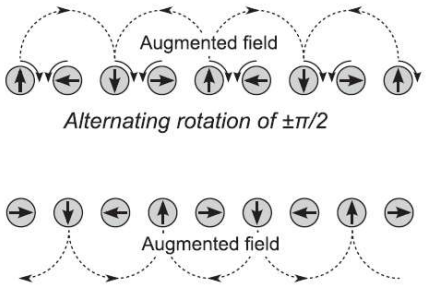

Figure 7 Adjustable linear Halbach array. The direction of the field can be continuously adjusted by alternately rotating all eight magnets 90 degrees. Adapted from [16]

By alternately rotating each magnet by 90 degrees, the direction of the field can be easily controlled. The author notes this configuration can be manipulated with a simple gear train and motor to adjust field direction. If a gear train is used, the torque profile required to overcome the interactions between the magnets is relatively small, and perfectly sinusoidal through the 90-degree rotation.

In this research, a new configuration was developed to produce a circular, adjustable, four pole magnetic field. The design uses 8 rod magnets and is inspired by the polarization pattern from [15] and the mechanical activation in [16]. Through experimentation, it was found that the direction of the field could be continuously controlled by rotating any four alternating magnets by 180 degrees in the same direction. Figure 8 shows a diagram of the new adjustable permenant magnet array. This arrangement leads to reduced number of moving parts and manufacturing complexity compared to [16].

One advantage is that any four alternating magnets can be used to control the array. If odd-numbered magnets are rotated through 180 degrees, the motor torque profile to overcome magnetic interactions becomes a skewed sinusoid with peaks at 45 and 135 degrees where the poles of roating magnets perfectly align with the fixed. These peaks can be elimintated by using the even-numbered magnets to control the array because their poles do not align with any other magnets through the activation rotation.

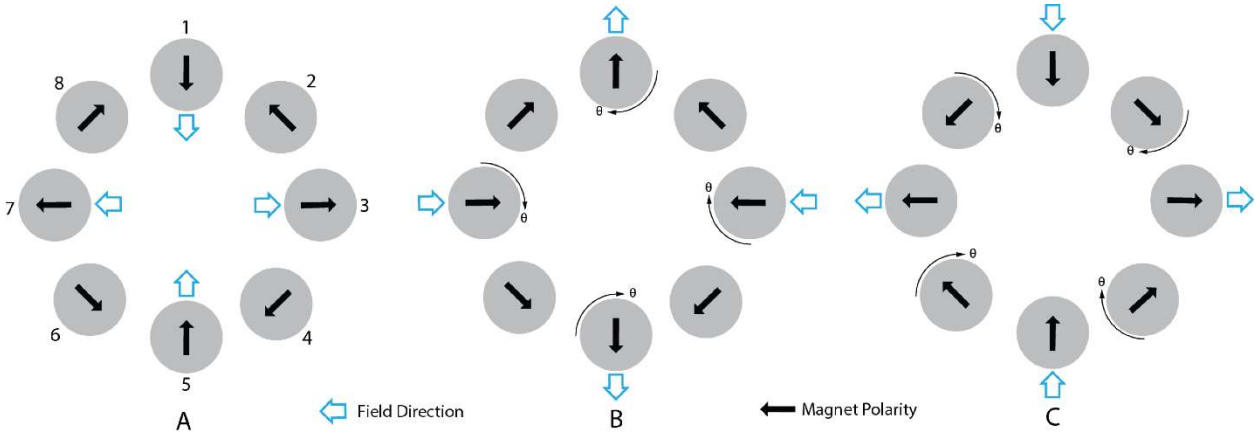

Figure 8 New simplified and controllable eight-rod circular Halbach array. In state *A,* all four poles are directed to and from the center of the array, resulting in almost zero flux on the outer surface. In *B*, magnets 1, 3, 5, and 7 are rotated 180 degrees, causing the poles to appear on the outer surface. The same result can be achieved by rotating the 2,4,6,8 magnets by 180 degrees and shown as state *C*.

Figure 9 shows flux simulations of the new adjustable array. When magnets 1,3,5 and 7 are in the orientation shown in Figure 9.A, the outer surface contains almost no magnetic field. But when the magnets 1,3,5,7 are rotated 180-deg as shown in Figure 9.C, all the flux is directed to the outer surface and the device is in the ON state. By rotating the magnets partially as shown in Figure 9.B, we can achieve variable levels of activation in the outer surface. This is important because the MR-fluid will be on the outer surface of the array in the final device design.

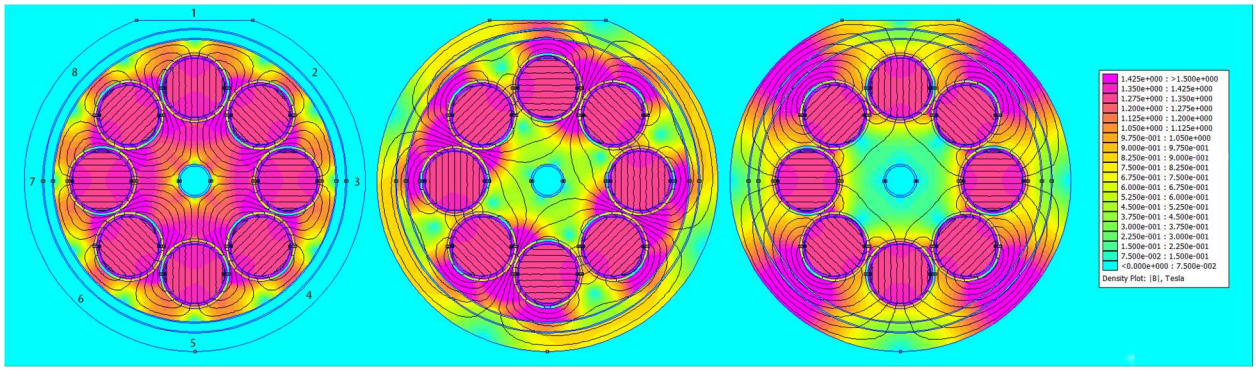

Figure 9 FEA simulations of the purposed device. In state A, the array is in the OFF state and most of the flux is directed towards the center. In B, the 1, 3, 5, and 7 magnets have been rotated 90 degrees showing a partially activated array. Finally, in C, the magnets have been fully rotated 180 degrees and the device is in the ON state.

2.1. Mechanical Design

A prototype magnet array shown in Figure 10 was designed and built. The array uses eight 0.5”D x 1”L diametrically magnetized N42 cylinder magnets. Four magnets of the array are rotated by a tiny motor.

The motor torque requirement is an important consideration in such a design. If the magnets greatly interact with each other, they would create a high torque to be overcome by the motor rotating them. Also, the magnet position needs to be measured for feedback control. An FEA simulation was performed to calculate the torque acting on each magnet throughout its rotation to leading to an estimated motor torque of 31 mNm.

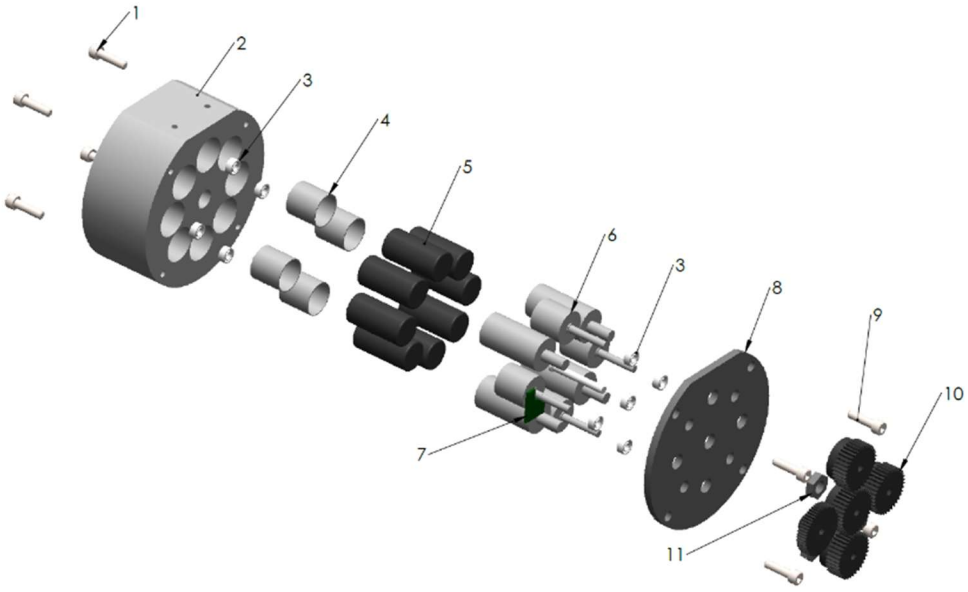

Figure 10 Prototype for proof of activation concept of the simplified eight rod adjustable circular Halbach array. Component details are described in Table 1.

Table 1. Simplified eight rod circular Halbach array activation prototype components

No.	*Description*	*Material*
1	Mounting Bolts	Steel
2	Main Housing	1018 Steel
3	*Bearings*	*Stainless Steel*
4	*Magnet Housings*	*1018 Steel*
5	*Magnets*	*N52 Nd2Fe14B*
6	*Magnet Housing/Gear Mounts*	*1018 Steel*
7	*Magnetic Angle Sensor*	*FR4*
8	*Front Cap*	*1018 Steel*
9	*Assembly Bolts*	*Steel*
10	*Fixed Magnet Nuts*	*Steel*

In the simulation, coercivity direction of the rotating magnets was parametrized in increments of ten degrees and solved for a range of 0 to 180.

The ideal motor should give the brake a time constant similar to conventional MRB designs with coils, usually between 50 and 110 ms. It would also provide enough torque to easily rotate the magnets, and possess minimal form factor. The mechanism was analyzed to find minimum torque and speed requirements to select a motor.

Assuming a trapezoidal velocity motion profile, the brake time constant can be approximated as:

$$\tau = 0.63\ t_{total} = 0.63(2t_{acc} + t_{mag}) \quad (6)$$

where τ is the time constant, t_{total} is the total time to rotate from 0 to 180 degrees, t_{acc} is the acceleration and deceleration time, and t_{mag} is the magnetic diffusivity time constant which was assumed to be negligible. The motor speed and acceleration is given by equation *7* and *8*:

$$\dot{\theta} = \frac{\theta}{t_{acc}} \quad (7)$$

$$\ddot{\theta} = \frac{\dot{\theta}}{t_{acc}} \quad (8)$$

where θ, $\dot{\theta}$, and $\ddot{\theta}$ are the rotational displacement, velocity, and acceleration of the movement respectively. Finally, the maximum torque required of the motor is given by equation 9 [17]:

$$T_{min} = J_{ref}^{trans}\ddot{\theta} + T_{Load} \quad (9)$$

where T_{min} is the minimum torque needed to turn the magnets, J_{ref}^{trans} is the combined moment of inertia of the four rotating magnets, housings, and gears reflected to the motor shaft, and T_{Load} is the torque from magnet interactions and bearing friction. Equations 7, 8, and 9 were combined to

determine the minimum motor requirements for this application. Assuming a desired time constant of 75ms, we calculated that the motor must be able to supply at least 25mNm at 500 RPM. For the prototype, the most convenient motor mount location was on the outer housing shown in Figure 13. This would allow for simple wiring access and space for larger motors if required.

To measure array rotation position, two methods were investigated. The most obvious solution was to use an encoder on the motor shaft. While simple, the encoder adds volume and cost to the device, and usually needs an additional indexing sensor. A alternate approach was to use analog embedded absolute Hall-effect angle sensor. The sensor takes advantage of the diametric polarization of the magnets in the array to measure angle.

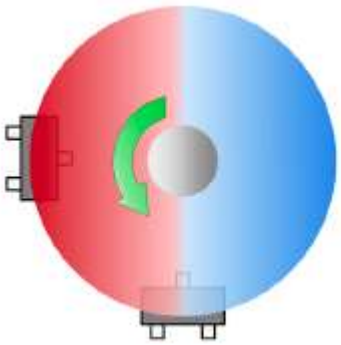

Figure 11 Texas Instrument's magnetic angle sensor configuration

The design uses two analog SOT 23 sized Hall effect sensors to measure the flux of the diametric magnet already existing in the device. As the magnet rotates, two sine waves are produced 90 degrees out of phase from each other. The angle of rotation is defined by Equation *10*.

$$\theta = \tan 2^{-1} \frac{B_1}{B_2} \qquad 10$$

Where B_1 and B_2 are the readings from each sensor. The arctan2 function is used because it can comprehend the sign variations of the flux readings and avoids divisions by zero. This sensor allows for absolute readings from 0-360 degrees, meaning it does not need any extra homing hardware for operation [18]. Additionally, it can be manufactured in house on 0.5mm FR4 making it remarkably thinner, cheaper, and with calibration, more accurate than encoders of comparable size.

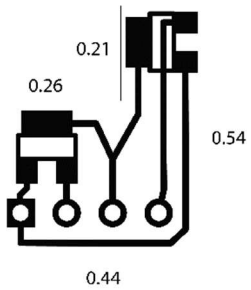

Figure 12 Magnetic angle sensor PCB with mounting pads for the A1302KLHT-T hall effect sensor. All dimensions are in inches

Figure 12 shows the PCB design and dimensions for the small Hall-effect encoder. The sensor could be made smaller in future embodiments but was enlarged for ease of use.

To verify FEA simulations and test the angle sensor a simple activation prototype was manufactured and shown in Figure 13 and the sensor location shown in

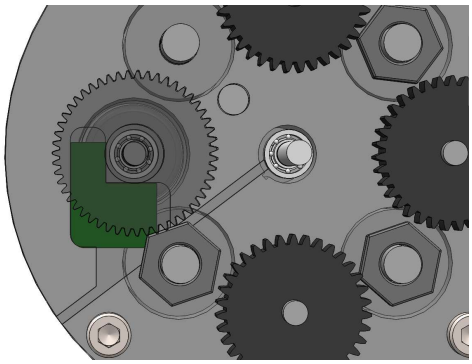

Figure *14*. This prototype did not contain any MRF or rotor, it was simply to verify the operation of the Halbach array proposed in Figure 8 and the mechanical control of the magnets with a micro-motor.

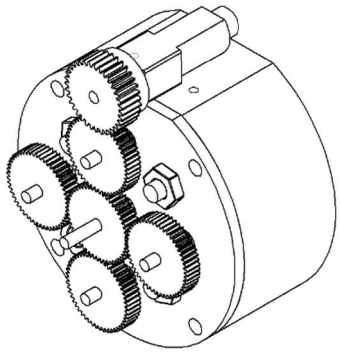

Figure 13. Sketch of eight rod circular Halbach array activation prototype including micro drive motor and gear train.

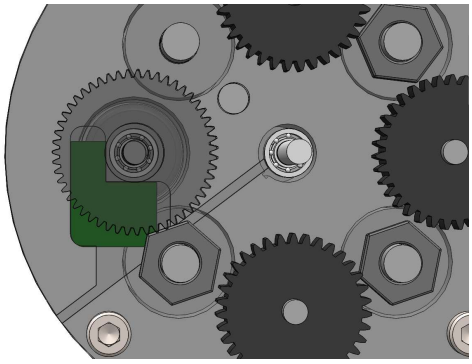

Figure 14. Hall-effect angle sensor location. PCB shown in green

The motor chosen to rotate the magnet array was a 75:1 Micro metal gearmotor from Pololu Robotics. It can produce 127 mNm with a maximum speed of 410 RPM and is available in a variety of gear ratios and motor voltages. It operates at 3-6 VDC with a stall current of 1.6A. It also includes a micro quadrature encoder capable of controlling the output shaft with a resolution of 0.4°.

One challenge with this design was mounting the magnets and aligning their magnetic polarizations with respect to each other. This was accomplished using a jig that allowed the magnets to interact with neighboring magnets, causing them to self-align. The north and south poles of each were then indexed and verified with a gauss meter. Using this method, the overall alignment accuracy was estimated to be within ±5 degrees.

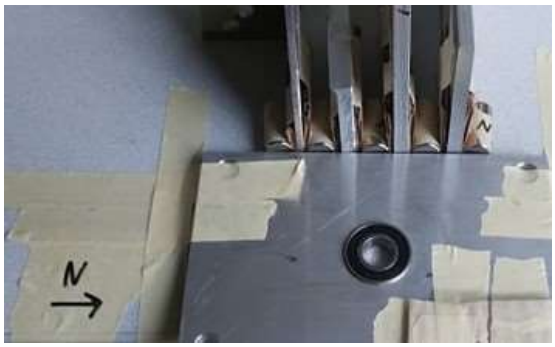

Figure 15. Jig to determine polarization direction for all eight magnets. In the jig, each magnet aligned its south pole with a corresponding magnets north pole. From there, the polarization directions can be easily marked on the face of each magnet.

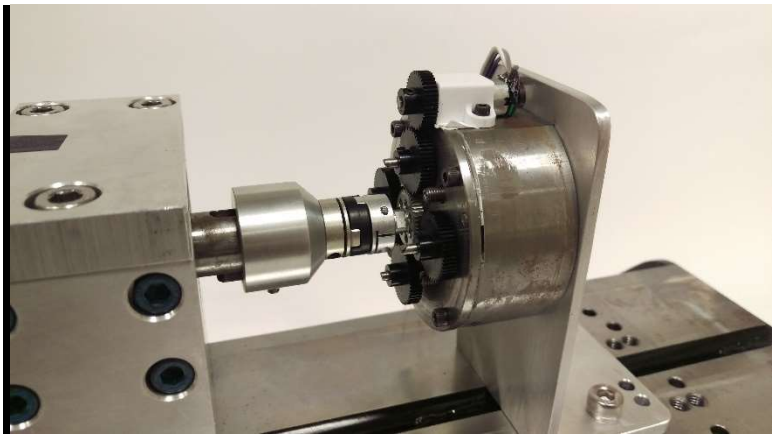

Figure 16 Completed circular Halbach array prototype mounted on a test bench.

For experimentation, the prototype was mounted to a test bench comprising large drive motor and gearbox, a torque sensor and high resolution optical encoder. Shown in Figure 17.

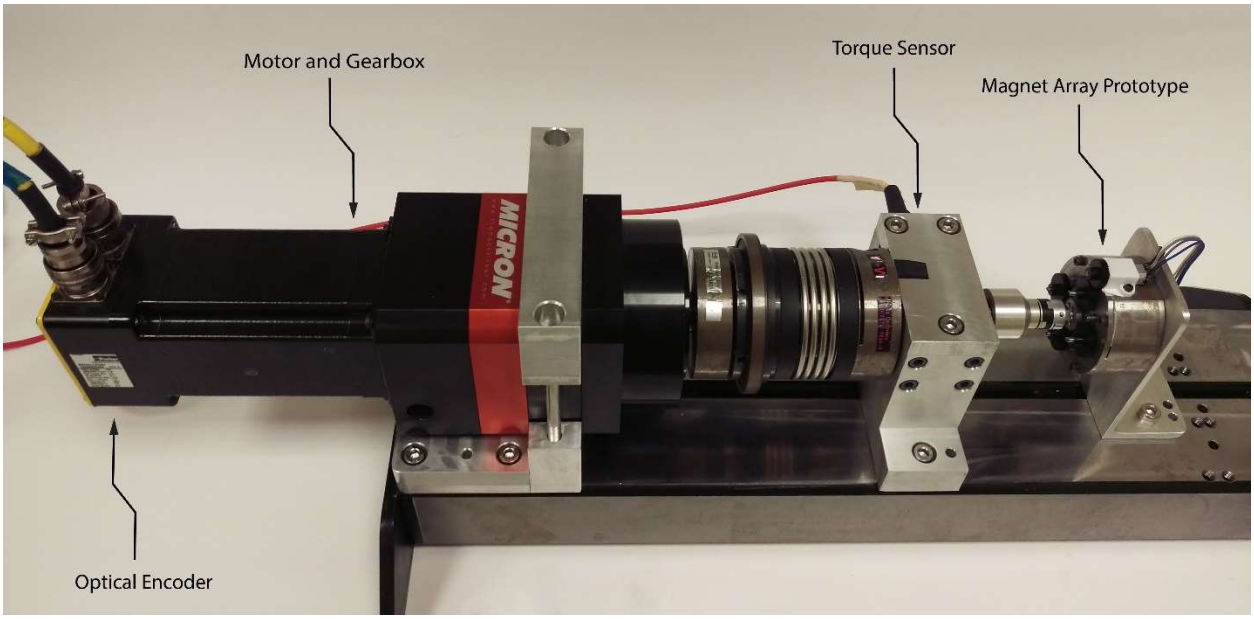

Figure 17 Complete test bench for measuring torque and rotation angle of activation prototype device with high resolution encoder.

2.2. Control Scheme

A unique challenge to this type of MRB was controlling the mechanical activation. The angle and speed of magnet rotation needed to be precisely controlled with the micro DC motor previously explained. It also needed to support variable speed and bi-directional activation. Fortunately, this type of system is well studied and a closed-loop Proportional-Integral-Derivative(PID) controller was implemented and shown in Figure 18.

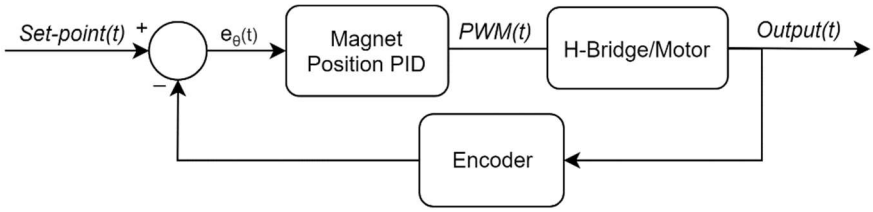

Figure 18. Closed loop PID control diagram for Halbach array activation

A Quanser Q2 data acquisition board was interfaced to an H-bridge (TJ15884) motor driver and the controller was implemented in SIMULINK.

2.3. Proof of Concept Experiments

Four experiments were performed to characterize the activation performance and verify simulations. In each case, the experiment began with the array in the off state, repeated four times, then averaged to produce uniform results. The first and most critical experiment was measuring the torque required to overcome interactions between the magnets while rotating from 0 to 180 degrees. To determine the maximum required magnet rotation torque, the odd-numbered magnets were chosen to activate the array. Refer to Figure 8 for numbering convention.

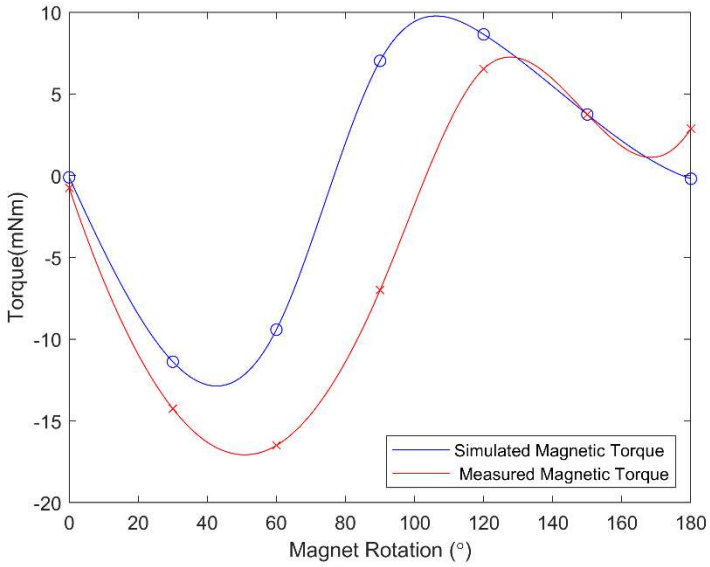

Figure 19 Measured and simulated magnetic torque on eight rod circular Halbach activation prototype including friction contribution

With the magnets installed, the rotation was discretized into 30 degree increments. At each step the high resolution encoder and the torque sensor of the test bench were used to record data. After comparing the experimental and simulation results, the rotational friction torque was estimated to be 18mNm and the maximum total torque was measured to be 34.1mNm at a position of 45° as expected. This is due to the poles of the rotating magnets directly aligning with the fixed ones at 45° and 135°. These alignments can be avoided by simply using the even-numbered magnets to activate the array. It is also noticeable the measured and simulated torque do not align well. The inaccuracy in the measured signal is mostly due to reading such small torques with the available sensor, which has a resolution of 5mNm with a 12 bit DAQ. Since the main goal of this experiment was to confirm that the proposed array requires very little torque to overcome magnetic interactions, this discrepancy is reasonable. The maximum torque required to rotate the magnets is very small and is well below the torque capacity of the selected motor.

The next experiment was to evaluate the performance of the magnetic angle sensor when embedded in the prototype. A pocket was machined into the steel endcap, allowing the Hall sensors to be aligned 0.02 inches from the surface of the number 7 rotating magnet (see Figure 8 for magnet numbering)

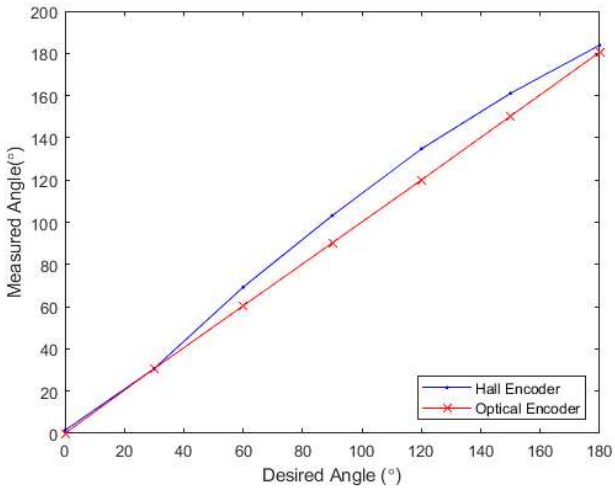

Figure 20. Measured angle with analog hall-effect angle sensor compared to high resolution optical encoder.

The encoder was successful in tracking the rotation angle, but was not completely uniform. Between 40 and 140 degrees, the measured angle was larger than the actual angle. The is most likely due to noise from the other magnets as the flux transitioned from the inward direction to outward. This could be accounted for in the future with a calibration curve or simply seating the sensor in aluminum rather than steel to reduce interference from other magnets. For simplicity it was decided to just use the encoder supplied with the micro DC drive motor but the embedded sensor might be employed in future designs.

The goal of the second experiment was to measure the magnetic flux density to verify FEA simulation results. A Hall effect sensor (A1302KUA) was placed on the outer surface of the prototype, at the

location shown in Figure 21. This location was chosen because it showed the greatest range of responses on the surface of the device.

Figure 21 Eight rod circular Halbach activation prototype including external hall sensor

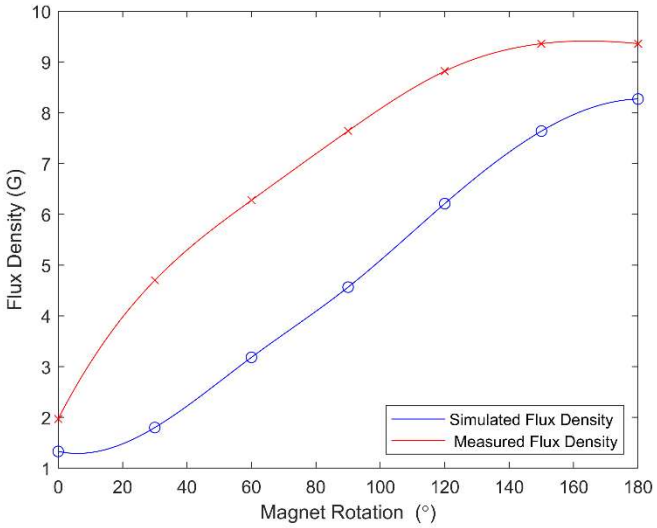

Figure 22 Measured and simulated magnetic flux density on surface of activation prototype

As shown in Figure 22, the measured flux was higher than FEA simulation predicted. This is probably due to the vector nature of magnetic flux density, making it difficult to accurately measure on a curved surface. The sensor only measures the component of magnetic flux traveling normal to its packaging at a point, so slight variations in sensor placement can result in large changes in readings. Also, the measured flux magnitude is very small (3-6 Gauss) making the measurements more prone to error. The experiment did however confirm the expected shape of the plot and activation of the array.

The third experiment was to measure the activation time constant using the micro gear motor for actuation. A closed-loop PID controller was employed to drive the motor using the pre-attached micro encoder for position feedback. After the PID gains were tuned, prototype was homed in the OFF state and the motor rotated the magnets 180 degrees to the ON state. The transient response is shown in Figure 23.

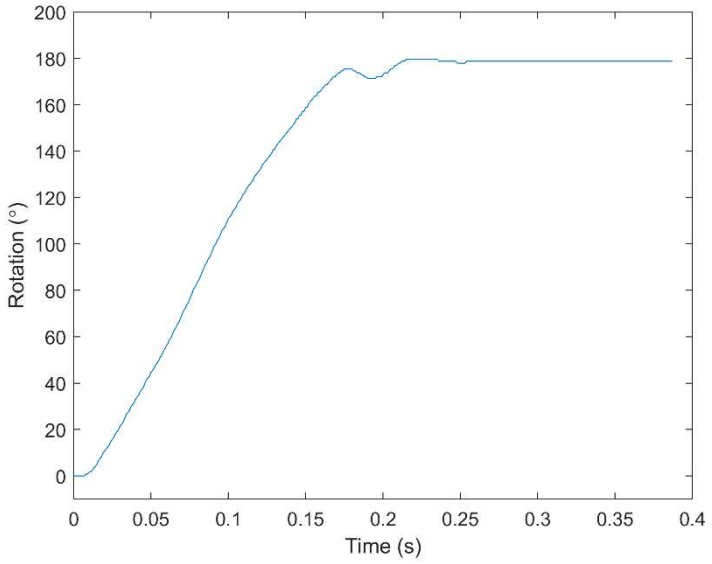

Figure 23. Activation prototype transient response of array rotation driven by micro DC motor

The time constant was calculated to be 95 ms. This is higher than the chosen target of 75ms. The difference was most likely due to not including motor efficiency characteristics in the model. In DC

motors the torque and speed are inversely proportional which becomes noticeable as the load torque approaches the maximum rated torque, significantly slowing the motor. The time constant could be improved by driving the motor with a higher voltage or purchasing a faster motor.

CHAPTER 3

MRB WITH SIMPLIFIED CIRCULAR HALBACH ARRAY

1.1 Validating Material Properties

The overall dimensions of the device are fairly limited, since it is constrained to the size of PMs readily available. To keep the overall diameter comparable to other MRBs, 0.5”D x 1”L N52 magnets were chosen. A housing was designed around the magnets, simulated using FEA, and internal dimensions adjusted for maximum ON and OFF state flux. The most critical dimension in the design is the distance between the magnets and the MRF. Since the array is not a perfect mono-pole, space was needed for residual leakage flux to flow without activating the MRF in the OFF state. In order to minimize the off-state torque and maximize the on-state torque, careful selection of core material with accurate material data was required.

Furthermore, it was found for the flux to avoid the MRF in the OFF state, each magnet needed to be approximately the same strength, to keep the array balanced. If unbalanced, the flux flows in a non-uniform lobe pattern, causing unwanted MRF activation. Other critical dimensions were the housing thickness and rotor shaft diameter. If the housing is not thick enough, flux flows parallel to the MRF rather than perpendicular, reducing the generated torque in the ON state. If the shaft is too large, the core saturates more rapidly, causing flux to leak through the MRF, increasing off state torque.

Due to the passive nature of this device and required balance between ON and OFF state torque, accurate material magnetic properties are essential for design. If parts of the brake saturate more quickly, or permanent magnet strength is different than expected it could ruin the balance between ON and OFF state torque. To ensure accurate material data for critical components, the BH curve of the core was measured along with the N42 magnets strength.

Since it is difficult to measure the BH curve of a material directly without disturbing the magnetic circuit, it was rather measured using an indirect approach according to the method described in [19]. To measure the curve, a sample was machined into a toroid and wrapped with two identical coils. An alternating current of 20V, 3A at 5Hz was applied to one coil for generating *H*, and the induced voltage in the second coil from the changing magnetic field was measured to calculate *B*.

The BH curve is created by plotting the magnetic field strength *H* generated by the first coil against the resulting magnetic induction (magnetic flux density) calculated with the second. Equation *11* was derived from Ampere's law and shows how to calculate *H* in an electromagnet.

$$H = \frac{I\,N}{L_c} \tag{11}$$

Where *I* is the current flowing through a coil, *N* is the number of turns, and *Lc* is the effective length of the core. This indicates if the physical dimensions of the core and the current being supplied are defined, the resulting H can be easily calculated.

B on the other hand is not as straightforward to measure. The fundamental equation to calculate *B* is Lenz's law and shown in Equation *12*.

$$E(t) = -N\,A_c\frac{dB}{dt} \tag{12}$$

Where B is the magnetic flux density, and *E* is the EMF generated in the second coil by the alternating magnetic field and *A*c is the crossectional area perpendicular to flux travel. Solving for *B* results in Equation *13*.

$$B = \frac{1}{-N\,Ac}\int_0^t E(t)dt \qquad 13$$

A schematic of the measurement setup can be seen in Figure 24. A function generator was used supply a sinusoidal 5Hz control signal to a current amplifier and an Arduino microcontroller was used for DAQ. By measuring the voltage across the 0.2 ohm resistor, the output current of the amplifier was found for calculating *H*. Likewise, the voltage of the output coil was monitored utilizing a voltage divider for over-voltage protection. The Arduino can only measure positive voltages but due to signal symmetry a complete sinusoid can be produced in post processing by mirroring the partial data about the X axis and shifting by half the period. The integration of E(t) can be performed live with an op-amp but for simplicity it was calculated in post processing using MATLAB. When *B* and *H* are plotted against each other, the full B-H loop is generated.

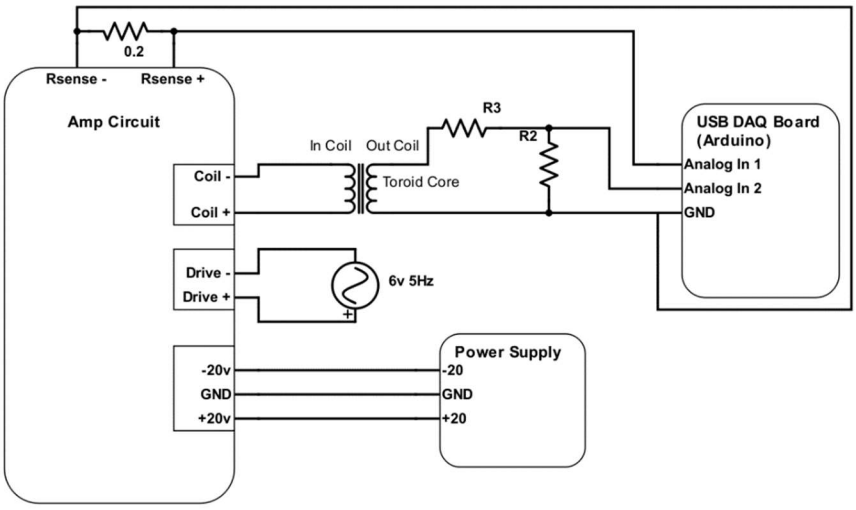

Figure 24. Schematic of BH curve measurement experiment

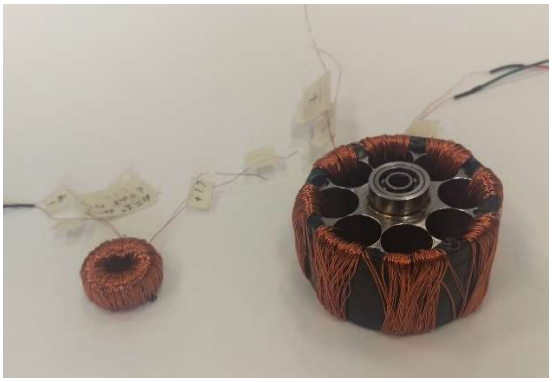

Figure 25. Example wrapped cores for measuring the BH curve. The torroid on the left was machined and wrapped specifically for the BH curve experiment and the sample on the right is the actual machined core for the MRB device wrapped with coils for the experiment.

Figure 25 shows two example samples for measuring the BH curve of a material. The simple toroid core on the left was machined specifically for the experiment; since it is smaller, it needed less turns to generate adequate flux density. On the right is the actual MRB core, wound with coils. Fortuitously, the core geometry had a closed loop toroid flux path that could be would with coils, allowing the BH curve of the final machined part to be measured as well.

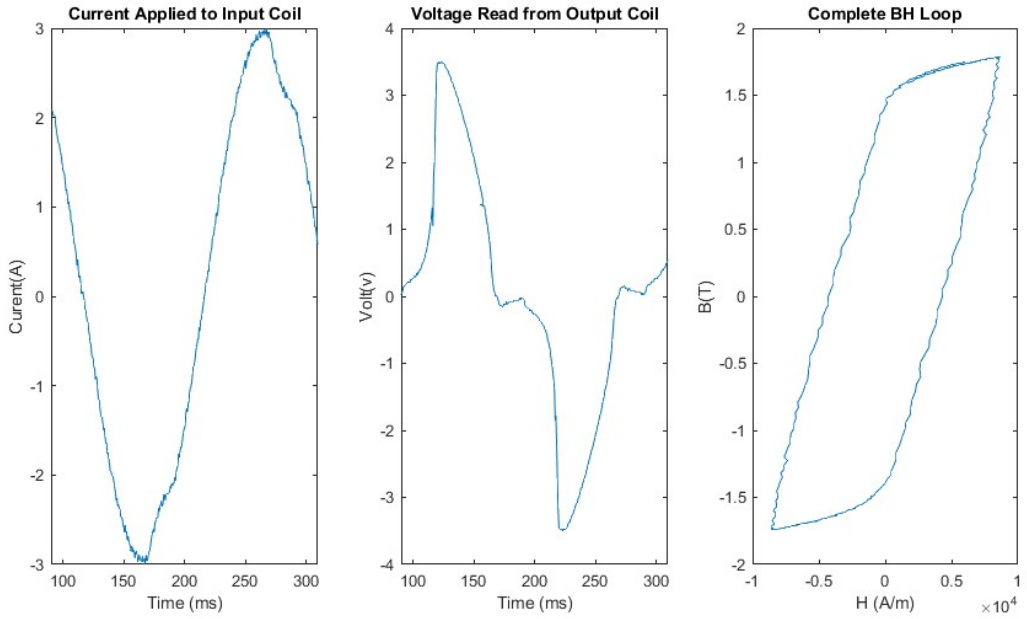

Figure 26. BH curve experiment results for a 1018 steel sample driven with 3A at 5Hz. A) The sinusoidal current applied to the drive coil, B) The resulting induced voltage in the output coil, C) The calculated BH loop

Figure 26 shows the resulting data plots for a 1018 steel sample, wound with 170 turns and driven with 3A at 5Hz. The driving frequency and number of turns was found experimentally to best measure the direct current(DC) magnetization curve, while still producing a large enough voltage for the DAQ to accurately read. If the drive frequency is set too high, the magnetic time constant of the metal begins to show, which slows down changes in the field strength. This does not allow the sample to completely saturate and results in a more circular shaped BH loop, known as the alternating current(AC) BH curve.

The first plot shows the sinusoidal current supplied to the drive coil from the current amplifier and the second shows induced voltage in the output coil from changing flux density according to Lenz's law described with equation *12*. Notice how it is not a perfect sinusoid like the drive current but warped,

which is a clear indication of nonlinearities in the sample. The final plot shows the complete BH loop produced using equation *13*, which has the expected shape for DC magnetization.

However, for simulations, only the initial curve is needed. This was found by averaging the positive magnetizing and demagnetizing portions of the full curve in quadrants one and two with the resulting curve shown below.

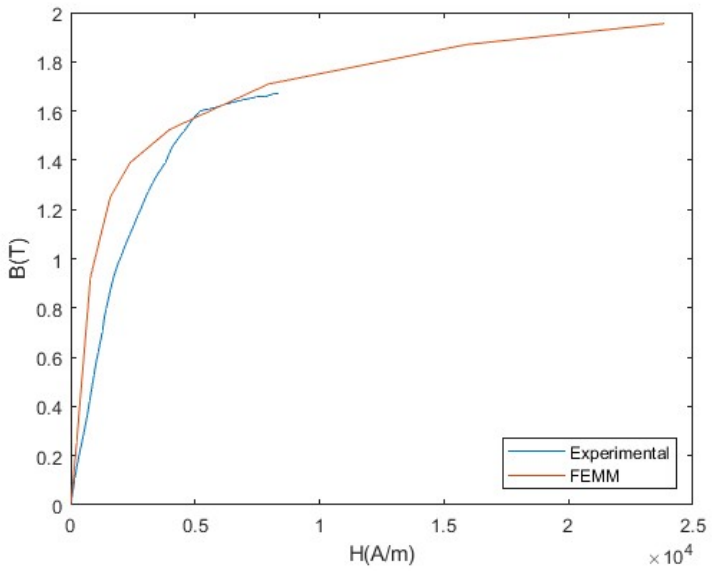

Figure 27 Measured BH curve of 1018 Steel using a 3A, 20v, 5Hz drive signal compared to BH curve from FEMM FEA software

As observed from the plot, the measured curve is a close match to the curve provided in FEMM FEA software. To verify, both sets of data were used to simulate the torque from an MRB, with results differing less than 2%.

Initially, the core material(part 4 in Figure 33) was chosen to be Annealed Carpenter Alloy 49 for its excellent permeability and low cost compared to other specialty soft magnetic alloys like Hyperco 50.

One downside of these high-performance magnetic materials is that they need to be carefully annealed to achieve optimal properties, usually in a dry hydrogen atmosphere or a vacuum. However, after machining and annealing it was found the BH curve did not match the datasheet. The annealing recipe was adapted from the datasheet, the only change being a vacuum atmosphere rather than dry hydrogen because of local equipment availability. The complete process and resulting BH curve can be seen in the appendix. For prototype reliability, the core material was switched to the more common 1018 steel however the BH curve was still measured to verify the datasheet. In future development of this device, a specialty alloy like annealed Carpenter 49 could be used to boost brake performance if accurate material data is available before designing.

The magnets were likewise measured using both a PCE-MFM-3000 Gauss-meter and a custom 3D printed jig(shown in Figure 28) with embedded Hall sensor so different locations could be measured accurately. Two locations were measured, one on the surface and one 1cm away from the surface. Each magnet was measured at these locations and compared to the datasheet and 2D FEMM FEA simulations of the same magnet. The first set of magnets measured were purchased as N52 grade magnets but when measured, they were actually 30% weaker than expected, much closer to an N32 grade. Another set of magnets were purchased from a different supplier as N42 grade. These were likewise measured using the same method, and after some slight adjusting to the datasheet's demagnetization curve for the FEA, they matched with a deviation of less than 1.5%.

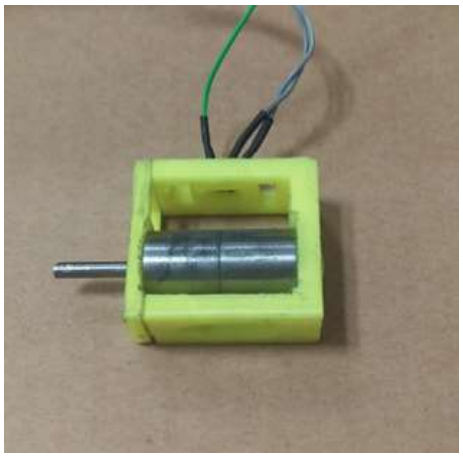

Figure 28. 3D printed jig with embedded hall sensor for measuring flux density a fix distance from the surface. The actual magnet is encased in a steel housing for mounting to bearings in the MRB.

1.2 SIMULATION MODELS FOR THE DEVICE

One of the more difficult aspects of this design was generating a reliable model to calculate the ON and OFF state torques for a given geometry. The shape of the field can be found analytically for highly simplistic geometries, but for most useful applications, FEA is employed to approximate the field. In typical MRBs a coil is used to generate the magnetic field for MRF activation. This usually results in a field where the normal and magnitude components are congruent when passing through the MRF, and can be easily approximated using 2D FEA because the single coil is axisymmetric through the length, affording simplifying assumptions in the model. When designing an MRF actuator, the direction of the magnetic field must be considered. For improved torque generation, the field component normal to the MRF surface should be maximized. In the proposed circular Halbach Array, the normal and magnitude components of the magnetic field are not equal when passing through the MRF and is not geometrically axisymmetric along the length. Furthermore, the end effects from the magnets also needed to be accounted for, so a new model was generated.

1.3 2D Approximation

The first method considered was using a 2D FEA model. The MRB was sliced down the center, exposing a cross-section of the device and simulated using Finite Element Magnetics software (FEMM). Figure 29 shows simulations of the MRB in three activation states.

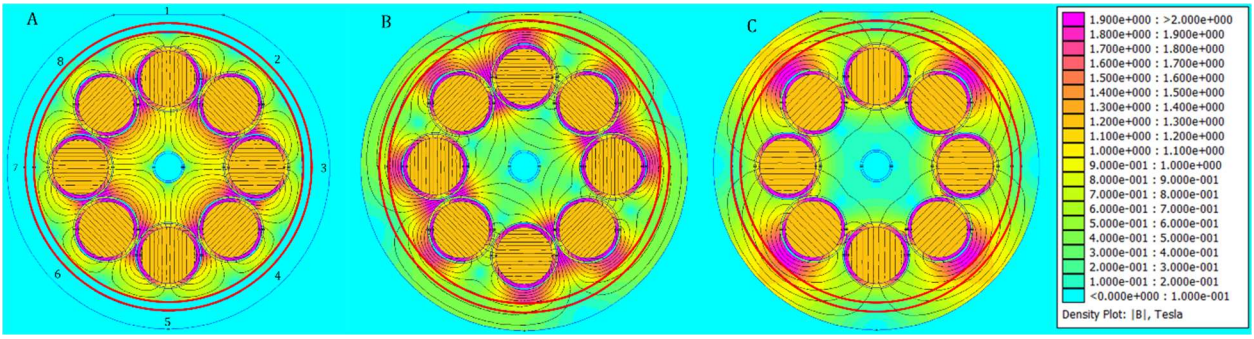

Figure 29 2D FEA planar simulations of the proposed MRB, red rings show the MRF layers. In state A, the array is in the off-state and most of the flux is directed towards the center. In B, the 1, 3, 5, and 7 magnets have been rotated 90 degrees showing a partially activated array. Finally, in C, the magnets have been fully rotated 180 degrees and the device is in the on-state.

The FEMM simulation only provides a 2D planar solution, but the end effects of the magnets need to be considered for the complete solution. For simplicity, the field was assumed to be constant along the length with the strength of the field dropping significantly at the ends. Using another FEA simulation along the length of the device, the effective length or usable length of the generated magnetic field was estimated to be 88% of the total length for the one-inch-long magnet. In a longer magnet, the end effects would be much less noticeable because there would be more surface area with a constant magnetic field in the center compared to the end diameter.

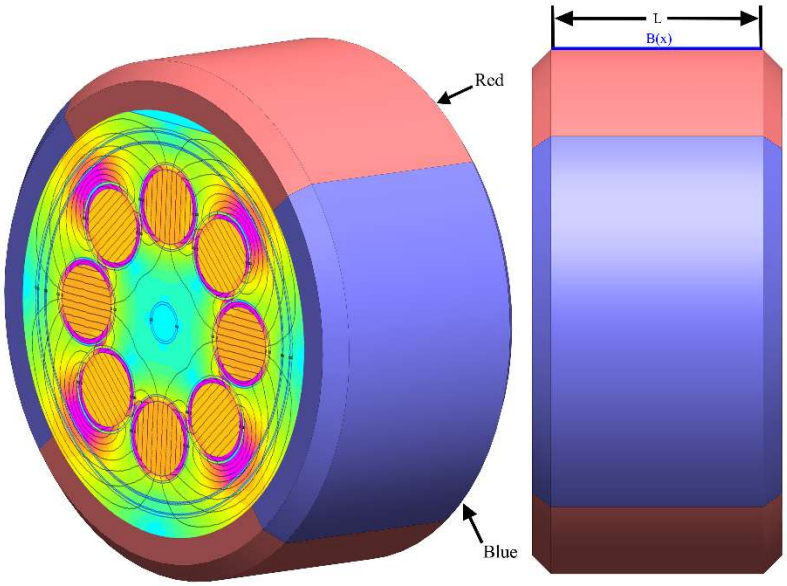

Figure 30. Approximated shape of normal magnetic flux density field through the rotor, generated by the array. The red and blue regions are the magnetic poles developed by the array. *L* is the effective length or usable normal flux along the length of the rotor

Figure 30 shows a simplified 3D representation of the normal flux through the MRF generated by the array. *L* is the effective length or usable normal flux along the length of the rotor, and *B(L)* is the value of the normal flux and assumed to be constant for the 2D approximation model.

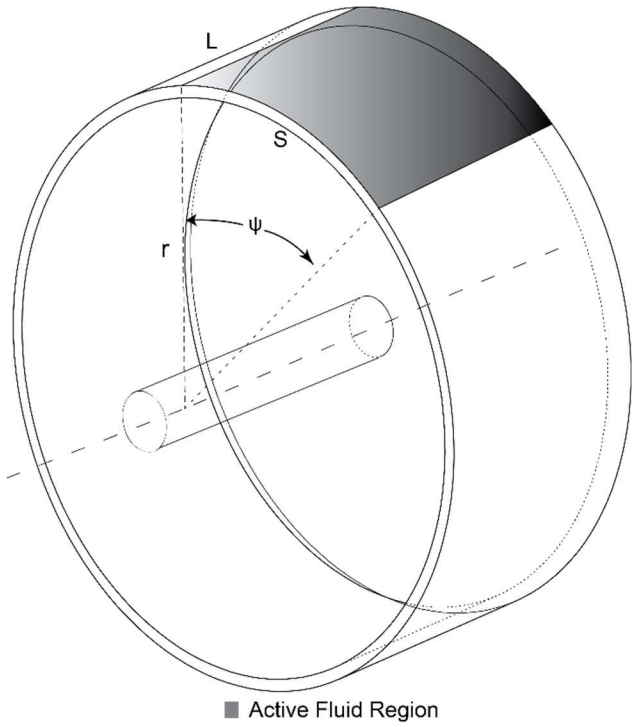

Figure 31 Sketch of inverted drum rotor, highlighting the active surface region for torque calculations. *L* is rotor length, *S* is arc length, *r* is surface radius, and ψ is arc angle

Using the simplified version of the Bingham-plastic model shown in Equation *5*, the force acting on the inverted drum can be found.

$$dF = \tau_{MRF}(\Psi) dA \quad (14)$$

$$dA = rL\, d\Psi \quad (15)$$

$$dF = rL\, \tau(\Psi)\, d\Psi \quad (16)$$

where *r* and *L* are the radius and length of the drum, Ψ is the angle of the arc segment being activated and *F* is the tangential force on the rotor. The torque can be found by simply multiplying by drum radius and integrating along the arc.

$$T = r^2 L \int_0^{\varphi} \tau_{MRF}(\Psi)\, d\Psi \qquad 17$$

$\tau_{MRF}(\Psi)$ was obtained from the data sheet for the MRF132 fluid by Lord Corp. Since the field produced by the array is not constant around the circumference of the rotor, it was necessary to numerically integrate $\tau_{MRF}(\Psi)$. This calculation was performed for both the inner and outer surfaces of the rotor and combined to calculate the total output torque of the device.

The 2D model was initially used to design the proposed device because of software availability and simplicity. However, after a prototype was built, the magnitude of the measured torque readings did not match the predictions made with the 2D model. To remedy this discrepancy, a more thorough model was developed using ANSYS Aim 3D to account for the losses along the rotor length. .

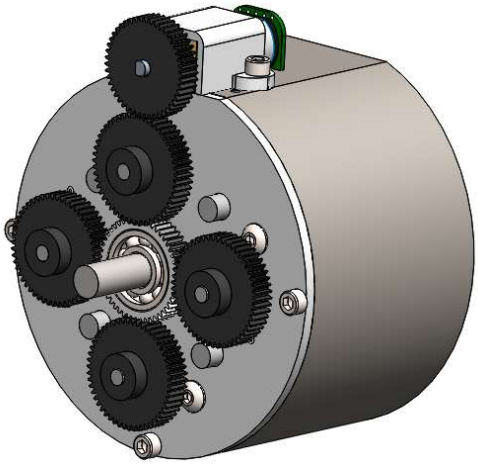

Figure 32. Proposed coil-less MRB using simplified eight rod circular Halbach array for magnetic activation

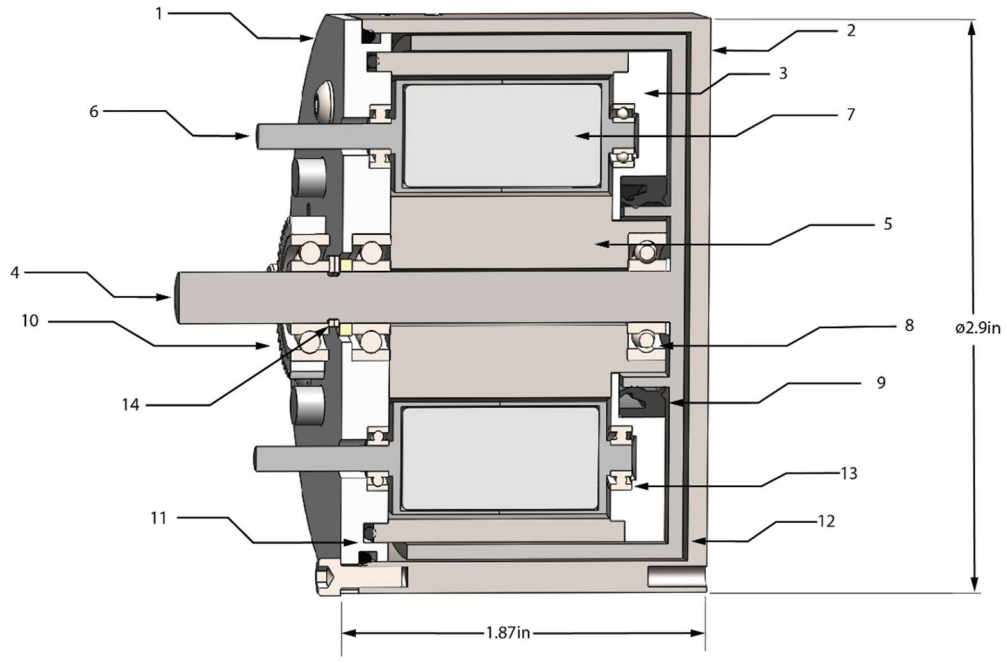

Figure 33. Section view and dimensions of proposed device without gear-train. Part numbers correspond to

Table 2

Table 2. Component descriptions for the proposed MRB described in Figure 33

No.	*Description*	*Material*
1	Outer End Cap	Aluminum
2	Housing	12L18 Steel
3	Inner End Cap	Aluminum
4	Rotor	12L18 Steel
5	Core	1018 Steel
6	Rotating Magnet Housing	1018 Steel
7	Magnet	N42
8	Rotor Bearing	Steel
9	Oil Seal	Rubber
10	Center Bearing/Gear	Steel
11	O-Rings	Rubber
12	MRF	MRF
13	Rotating Magnet Bearing	Steel
14	Snap Retention Ring	Steel

1.4 3D Approximation

The 2D model was initially used to design the proposed device because of software availability and simplicity. However, after a prototype was built, the magnitude of the measured torque readings did not

match the predictions made with the 2D model. To remedy this discrepancy, a more thorough model was developed using ANSYS Aim 3D to account for the losses along the rotor length.

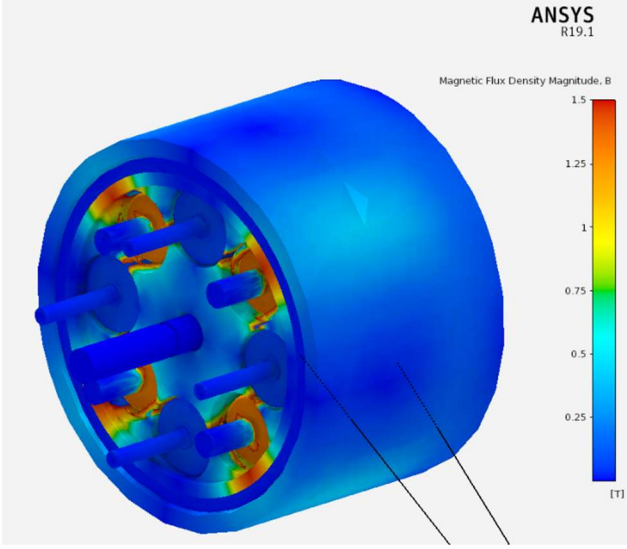

Figure 34. 3D FEA simulation in with Ansys Aim showing the magnitude magnetic flux density in the proposed device.

Using the 3D simulation, it was found that the flux along the rotor was not constant as previously assumed, but decayed along the rotor length.

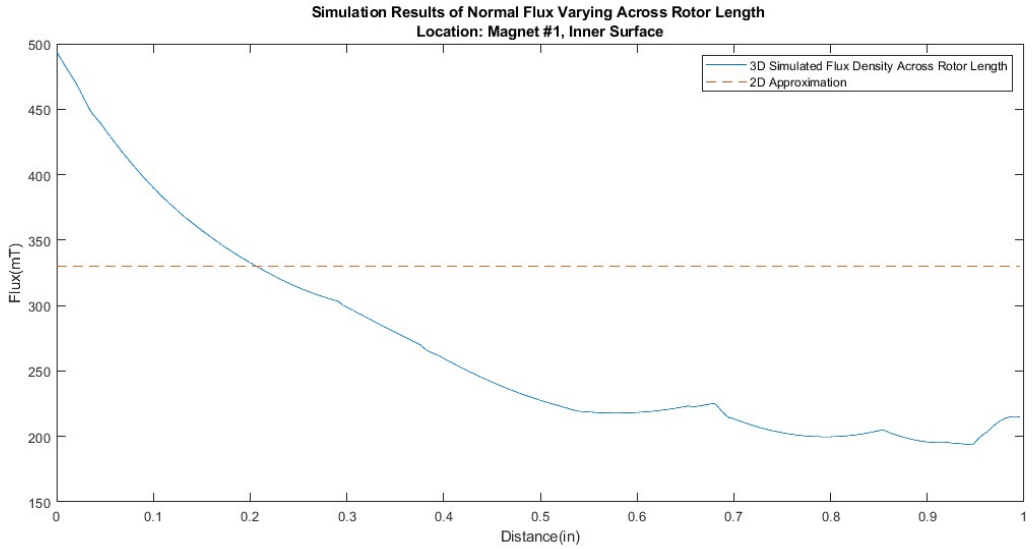

Figure 35. 2D and 3D Magnitude flux density simulations compared across the length of the rotor. Notice how the solid line decays while the dashed line is constant. For reference the datum is where the core and inner endcap meet (parts 3 and 5 shown in

Table 2)

As previously mentioned, the magnetic field can be described as a 3D vector. In MR devices the critical field component is the flux traveling perpendicularly through the MRF. Figure 35 shows how the normal flux decays along the length of the rotor on the inner surface directly above magnet 1. This location was chosen because the normal and magnitude flux density are the same at this location. The dashed line shows the expected constant 2D flux when neglecting 3D effects, this difference is why the 2D model was not accurate enough for simulating the device. To include this decaying property of the field, a new field shape approximation was generated and shown in Figure 36.

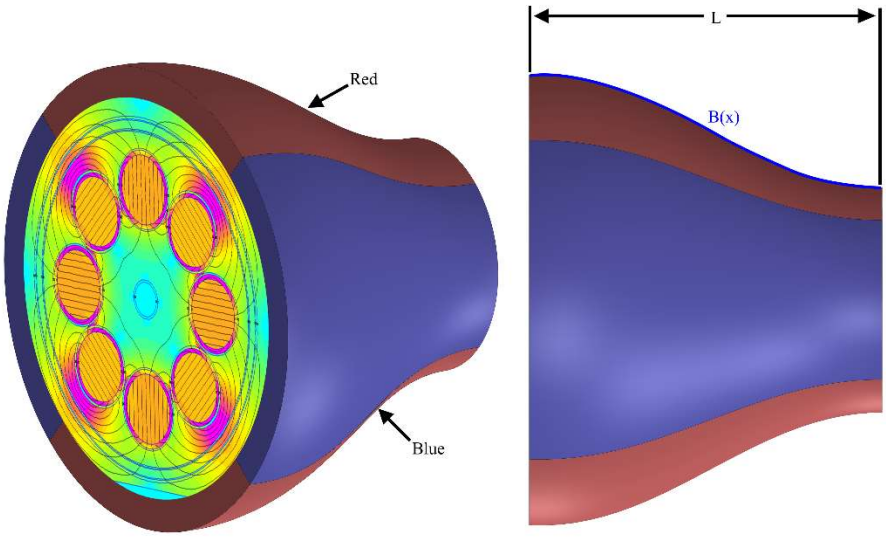

Figure 36 Approximated shape of normal magnetic flux density field through rotor generated by the magnet array. *B(L)* is how the normal flux decays along the rotor length and was found using the 3D FEA simulation.

To keep the model solvable with available software, the field was assumed to decay at a constant rate down its length such that B(L) is the solid line in Figure 36. In this way, the 2D simulations can still be used to calculate how the flux changes around the circumference of the rotor, but a scaling value *K(x)* is applied at discretized *dx* intervals to account for 3D losses.

$$K(x) = \frac{B_{3D}(x)}{B_{2D}} \tag{18}$$

where K is the scaling factor, $B_{3D}(x)$ is how the flux changes along the length of the rotor, and B_{2D} is the ideal 2D flux, (the solid and dashed lines respectively in Figure 35). Equation *17* can then be modified to include the scaling factor, resulting in a surface integral across the rotor to calculate torque and illustrated as:

$$T = r^2 \int_0^{2\pi} \int_0^{L} K(x)\tau(\Psi)\, dx d\Psi \tag{19}$$

where *T* is torque, *r* is rotor radius, *L* is total core length, *K* is the decay scaling function, $\tau(\Psi)$ is the fluid shear stress, *x* is the distance along the rotor length, and Ψ is the arc angle, just as in Figure 31. As shown in the following experiments, this model could predict the output torque of the device much more accurately than the original 2D model.

CHAPTER 4

EXPERIMENTS AND RESULTS

To help characterize the proposed device, five experiments were performed. The goal was to illustrate the controllability, ON and OFF torques, dynamic response, and conditions required to manipulate the Halbach array. The same test apparatus outlined in Figure 17 was used and the simple PID controller in section 2.2 was utilized to control the rotational position of the micro motor and magnets. All MRF torque experiments were performed with the rotor driven at 2RPM to avoid any shear thickening effects in the fluid.

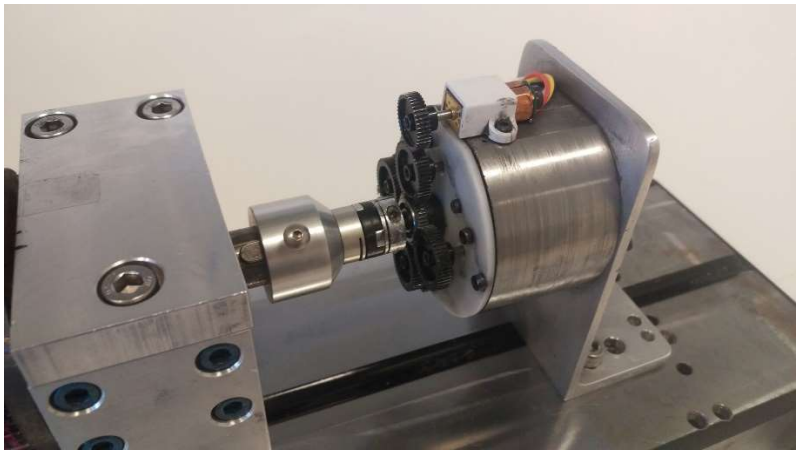

Figure 37. Proposed Circular Halbach Array activated MRB mounted on test bench.

4.1 Braking Torque

The first and most critical experiment was determining the controllability, OFF and ON torque for the device. This was accomplished by placing the array in the off configuration and measuring the torque as the array was slowly rotated to the ON configuration using the micro motor.

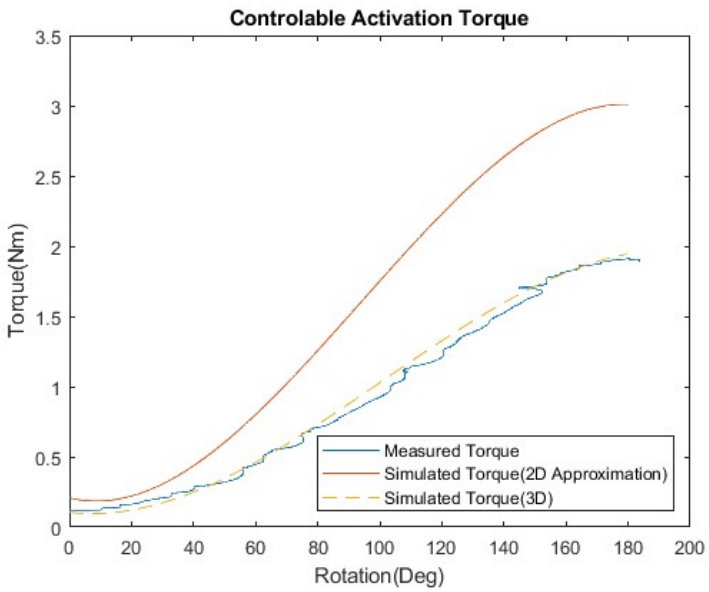

Figure 38. Measured controllable torque of the proposed device compared to the initial 2D model and the more thorough 3D model.

As observed, the 2D model overestimates the output torque by about 1Nm but does capture the correct shape. This model assumes the normal flux generated by the array to be symmetric and constant across the effective length of the magnet as illustrated in Figure 30. The updated 3D model was able to predict output torque much more accurately by accounting for the decaying field along the length of the rotor which was present in the actual device.

4.2 Hysteresis

One important factor when designing any magnetics based actuator is the hysteresis effects present in the device. Magnetic hysteresis is a phenomenon observed when a ferromagnetic material is placed in an external magnetic field and the atomic dipoles of the material align themselves to the field, resulting in residual magnetization when the field is removed. This is typically not desirable as it is more difficult to use simple open-loop control to drive the device.

For this experiment, the array was initially placed in the OFF position and rotated at a rate of 90deg/s to 180 degrees or the fully ON position, rotated in the opposite direction to -180 degrees, then back to the starting position.

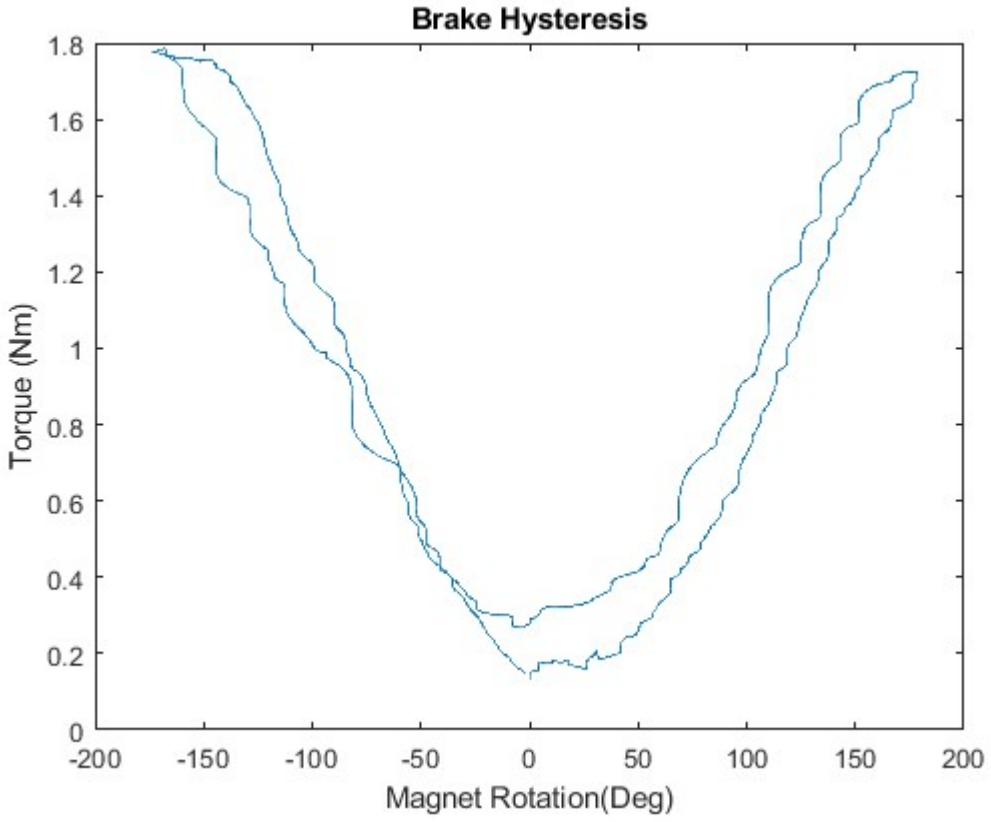

Figure 39. Hysteresis of the brake

The plot clearly shows some hysteresis in the device but is reasonable for this type of device. The hysteresis effects could be reduced by using a high performance alloy like annealed Hyperco 50 which has a sharper BH curve when compared to the 1018 and 12L14 steel used in this device.

4.3 Dynamic Response

One of the more concerning characteristics of this device was the transient response or the time required to transition from fully OFF to fully ON. This was measured for both the mechanical activation

and the MRB torque by subjecting each to a step input and measuring the time required to reach 63% of their respective final values, otherwise known as the time constant of the devices. The reason for interest in the parameter is because most MRBs use high-power, solid-state coil activation where this devices uses low-power mechanical activation which is inherantly slower. As such, the low power requred to run the proposed device was achieved by sacrificing rapid response times.

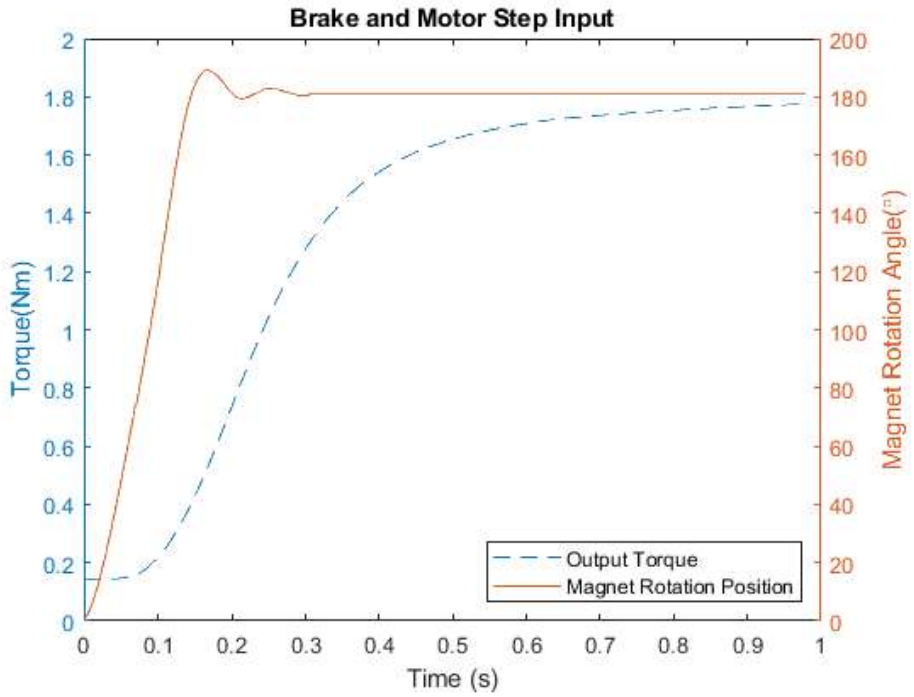

Figure 40. Step response of the proposed device. The dashed line is the torque output of the device with a time constant of 194ms and the solid line is the magnet rotation position with a time constant of 97ms.

Figure 40 shows a plot of the step inputs for the micro motor and the actual MRB. One of the noticeable features is how the torque lags behind the mechanical rotation of the magnets. The time constant of the for the magnets to rotate is 97ms which is not unreasonable when driven by an inexpensive micro DC servomotor. The torque on the other hand has a time constant of 194ms, which is a significant increase. This is most likely due to the magnetic diffusivity or diffusion time of the magnetic circuit.

Magnetic diffusion time is the time required for the flux density *B* to rise at least 63% of its final value when a field *H* is applied to a material, in this case from the permanent magnets. This value can be analytically determined for simple one dimensional, linear geometries. For example, a device with cylindrical actuator such as a solenoid, and B only varying over the radius:

$$\tau_m = \frac{\mu\sigma R^2}{2.4048^2} \qquad 20$$

where τ_m is the magnetic time constant, μ is the linear permeability, σ is electrical conductivity, *R* is the cylinder radius, and the value 2.4048 is the root of the first-order Bessel function [20]. For more complex geometries, with non-linear material properties and non-uniform magnetic fields, such as in the proposed MRB device, a non-linear, transient, 3D FEA solver is needed to accurately estimate the diffusion time. Unfortunately, access to this type of software was unavailable to our lab at the time of writing so was unable to investigate further. It can be deduced however based on the hyper-simplified cylinder magnetic diffusion equation above, that the amount of ferromagnetic material in the magnetic circuit strongly effects the diffusion time for any given geometry.

4.4 Curve Following

Another defining characteristic of MRBs is how well the output torque can follow a desired torque profile. To accomplish this a PID controller with feed forward was developed in Simulink. Initially a standard PID was used to control the torque but it was unable to keep up with rapid changes in set-point torque, so the velocity feedforward was introduced which allowed for a much faster response.

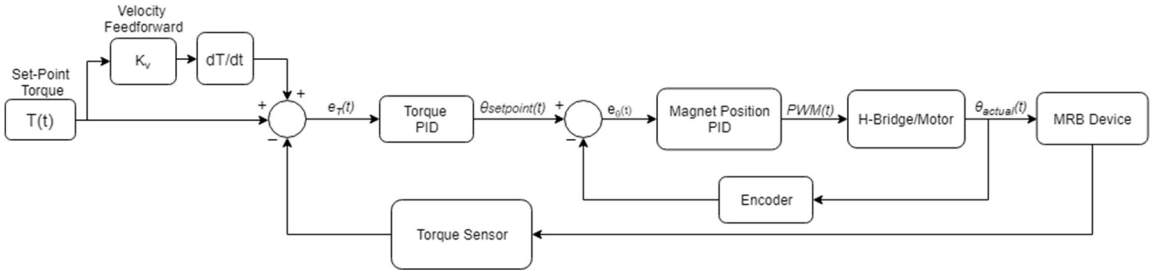

Figure 41. Velocity feedforward PID controller for MRB torque curve following.

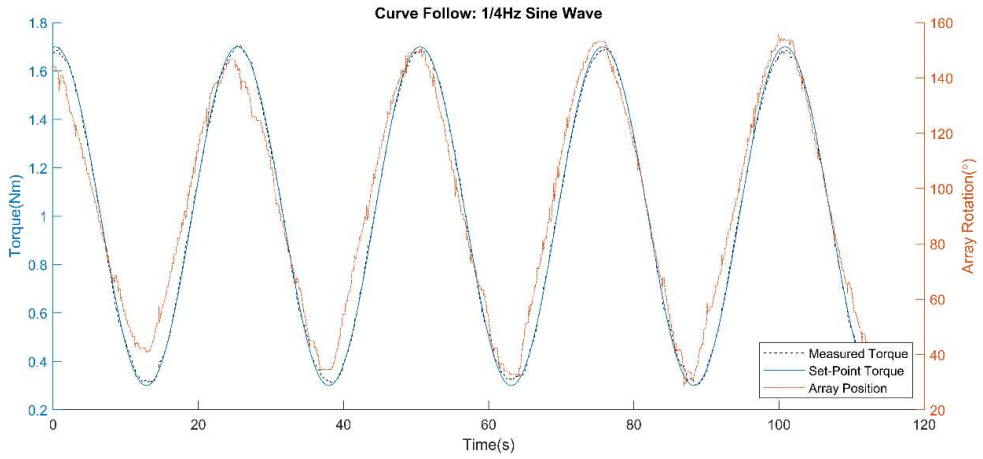

Figure 42. Sine wave torque following of proposed MRB

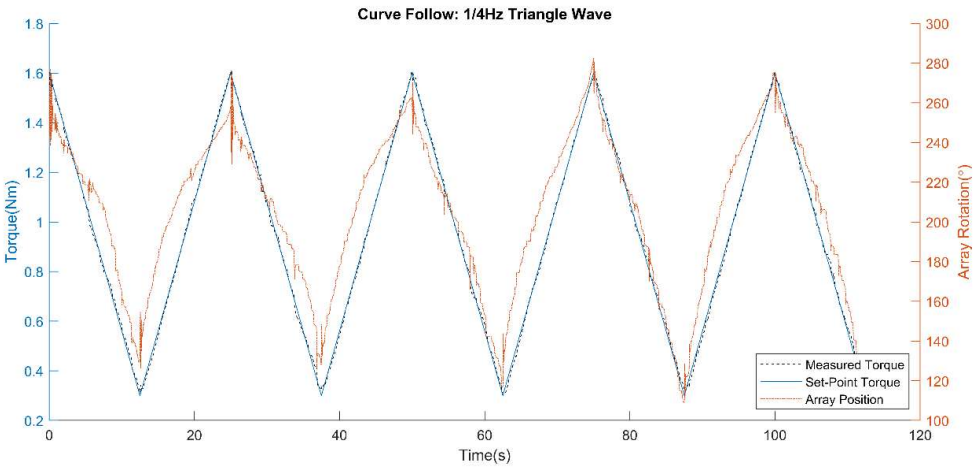

Figure 43. Triangle wave torque following of proposed MRB

As observed, the device was able to successfully follow both smooth and non-continuous curves when paired with an appropriate control system.

4.5 Halbach Array Rotation Torque

One experiment unique to this device is determining the torque required to overcome magnetic interactions and rotate the circular Halbach array for activation. In many configurations of magnetic arrays, the interactions are so great that assembling them is difficult and are prone to cogging torque such as in electrical motors with permanent magnets. From the proof of concept experiments outlined in section 2.3, the torque should be small.

To capture this data, the torque sensor on the test bench was attached to the center connecting gear of the array. The gear train has a 1:1 ratio so when the large drive motor turns, the magnets in the array likewise turn the same amount. The angle of rotation was monitored using the drive motor's built-in optical encoder.

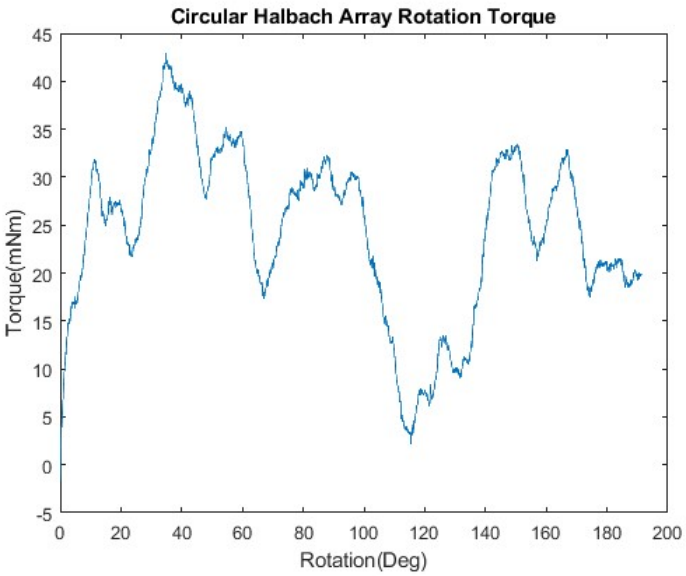

Figure 44. Torque required to rotate the proposed circular Halbach array and overcome magnetic cogging

The plot shows raw torque data from the experiment. While the signal is noisy, it does confirm the expected spikes in torque around 45 and 135 degrees as explained in section 2.3. The noise in the signal is mostly due to trying to read such small torques with the available sensor which has a resolution of 5mNm with a 12 bit DAQ.

The main goal of this experiment was to confirm that the proposed array requires very little torque to overcome magnetic interactions. With a peak of only 43mNm to overcome magnetic interactions and bearing friction, it is easily controllable with a small motor. It must be noted that this is only true for rotational motion about the axis of each magnet and they do have a strong lateral attraction to each other, so they must be held firmly in place with bearings to only allow rotation.

One of the unforeseen advantages to this design is the ability leave the array activated at any point through rotation with no continuous power required. The friction in the bearings is enough to overcome

minute magnetic cogging. As a result, power to the servomotor is only required when the torque needs to change value; when the desired torque is constant, the motor can completely shut off.

4.6 Power Consumption

As stated at the beginning of this paper, one of the primary goals of this work was to design a low power MRB for extended use. Since there are no coils in the MRB, the only power required is for the micro servomotor controlling the rotational position of the array. To measure power draw of the motor, a resistive based current sensor like the one shown in Figure 24 was used to monitor current draw and voltage across terminals of the motor for one step rotation of 0 to 180 degrees. Using the current and voltage data with elementary circuit equations, the power draw and total energy capacity for one activation were calculated.

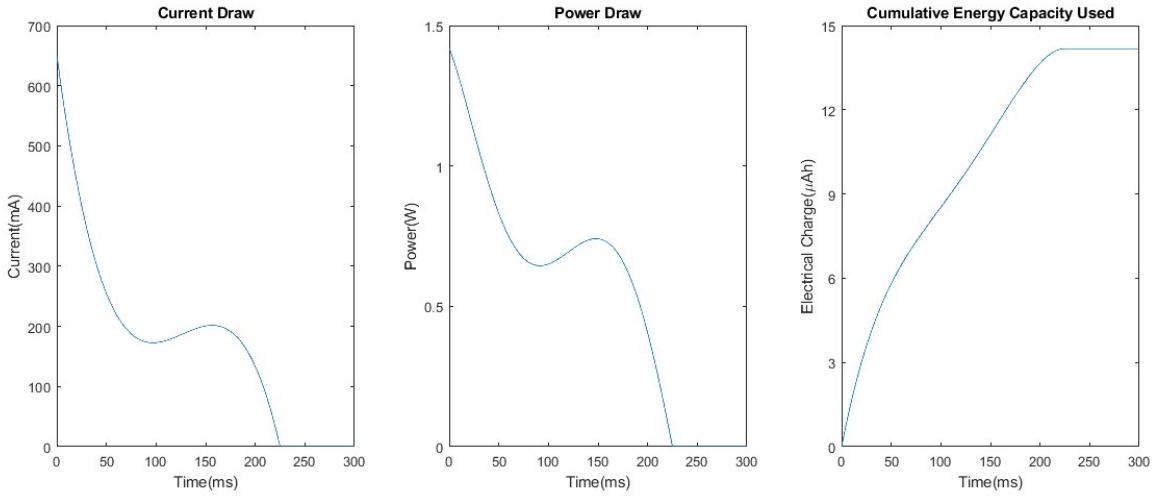

Figure 45. Measured electrical requirements to drive micro servomotor for one step input of 0 to 180 degrees.

From the center plot, it is observed the maximum power draw is 1.4W when the rotation starts. It then steadily declines until the motor start slowing down, about half way through the rotation where it

increases slightly for about 50ms then drops off completely when rotation is complete. By integrating the power draw over time the total energy capacity used was found and shown in the third plot.

For the proposed MRB, the consumed energy capacity for one rotation is a more reliable metric to characterize the device since power is only needed when the desired torque output value is changed. It could potentially sit for hours in the fully activated ON state requiring no power, unlike traditional coil based devices.

To illustrate the power advantage of this device, assume a small 7.2V 500mAh battery is used to power the MRB and torque changes are desired every two seconds. Under these conditions, the device could potentially run for 21.8 hours. Even if the worst case scenario was encountered and the torque needed to be changed to fully ON and fully OFF continuously, it could run for 2.2 hours. Compare this to a typical coil based MRB [3] that requires 16W and 2.22A if supplied with 7.2V. Using the same battery, it could only last 13.5 minutes.

CHAPTER 5

DISCUSSION

5.1 Comparison to State of the Art

As the case in other MRB research, it is often difficult to compare a new device with established, because they are often unique in purpose and design. In the case of the design proposed in this paper, the goal was to investigate low power options not previously researched, where many other designs focus on optimizing output torque and brake volume. In an effort to relate the Halbach array based device, MRBs developed in the past six years were analyzed and reduced to four defining ratio-metric parameters. To keep scoring unbiased, two metrics describing power usage, two describing torque performance were considered and shown in

Table *3*. The dynamic response would also have been included but there was not enough data provided in the literature for complete scoring.

Table 3. Design and performance comparison of MRBs

	Device	T_{on}/T_{off} -	T_{on}/Vol kN/m^3	P_{on}/Vol kW/m^3	P_{on}/T_{on} W/Nm	Time Constant for reference ms
1	**Proposed Device**	24.4	9.2	0.0	0.00	190
2	Disk Brake [21]	-	3.2	-	-	-
3	T Rotor Design [22]	8.2	-	-	-	-
4	Dual Disk for Haptics [23]	-	13.2	-	-	-
5	Drum w/Coil and Permeant Mag [11]	9.3	19.4	131.7*	6.8*	-
6	T Rotor [3]	32.5	64.1	157.8	2.5	75
7	Disk w/Coil and Permeant Magnet [24]	41.3	27.6*	-	-	-
8	Multi-Pole EM Brake [2]	-	13.1	15.4*	0.2*	-
9	Multi Disk [5]	96.2	16.2	5.4	0.3	-
10	Multi Cylinder [6]	176.0	48.1	172.4	3.6	50
11	Drum w/hybrid activation [25]	-	-	-	2.1	100
12	Multi-pole and dual-gap [10]	19.5	28.8	12.8	0.4	-

13	Multi-pole and dual-gap [2]	13.8	25.7	35.7	1.4	70
14	LORD Steering Unit 5Nm [7]	10.0	19.5	39.0	2.0	-
15	LORD Steering Unit 12Nm [7]	12.0	6.8	14.0	2.1	-

* Value not explicitly provided and estimated based on other information

These parameters were then assigned a score against each other on a scale from 0 to 10. In each category the brake with the best performance was given a perfect score of 10 and the worst 0. All other scores were linearly interpolated between those two values. In cases where one or two pieces of information were not provided in the literature, a nominal score of 5 was assigned to each parameter. If there were three missing, each was given a score of 10/3 as to not distort the scoring with missing information. Finally, the scores for each category were summed and compared in Figure 46.

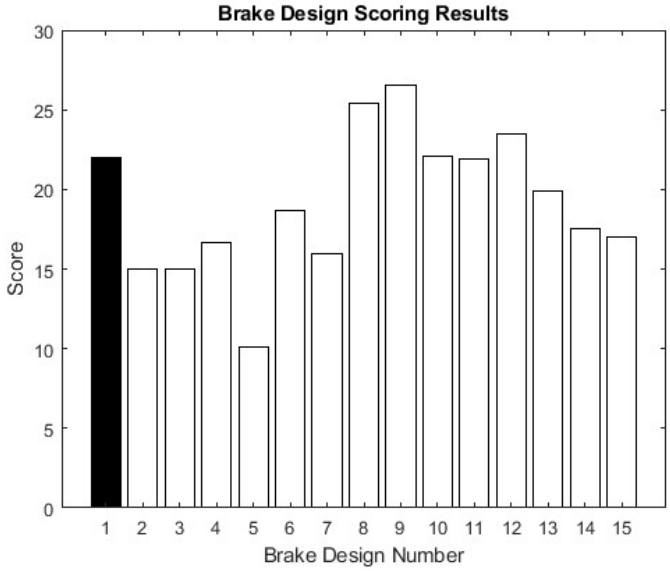

Figure 46 Scoring results for MRBs in the literature compared to the proposed device shown with the solid bar. Maximum score is 40pts. This plot is linked to table above

The proposed new device shown as number one on the bar plot above scored admirably when compared to the literature. Its main shortcomings are delivering relatively low torque for its size and a

slower time constant when compared to other devices. It does however pose many advantages over MRBs previously studied.

The most notable feature is being able to operate on minimal power, only requiring energy when changing the desired torque. Furthermore, it is continuously controllable and can be left at any activation state with no maintenance power needed. While there are other designs that scored higher overall, they required an average of 19 watts for continuous operation. Previous designs incorporating PMs required coil power to counteract the PM field for deactivating the MRF and additional power for maximum torque [11]. While there have been other PM only MRBs studied, we could find none capable of variable torque, operating only in a Boolean state and requiring external pneumatic equipment for operation [12]. In contrast, this device can easily be controlled with a simple, low power microcontroller and small battery.

This marks a distinct improvement in the state of the art MRB technology. Furthermore, the device incorporates a unique activation mechanism, not previously studied in the context of MRBs. This activation scheme enables the MRB to be left at any activation state with no applied power. Additionally, since this design does not use coils, it is not susceptible to joule heating which can reduce MRF performance when activated for prolonged periods of time.

While the mechanically activated design is highly power efficient, it does present a few challenges. Most apparent is the need for moving components. Traditional coil based brakes operate in the solid state resulting in rugged designs with faster time constants. The permanent magnets also require a more specialized geometry than coil based brakes for activation, proving to be a limiting factor when selecting rotor styles.

5.2 Future Improvements

When designing the proposed device, an effort was made to choose dimensions and materials such that torque performance and size would not suffer greatly when implementing the mechanically activated, permanent magnet array. That being said, there is definitely room for improvement. To give design insight for future work two influential dimensions were parameterized individually and simulated using the 3D FEA model method described in section 1.4.

The first dimension was the core's (part 5 in Figure 33) diameter. The dimension directly relates the distance of the magnet surface to the MRF. It was initially set to 2.4 inches then reduced to 2.2 and the torque was found for the resulting ON and OFF states. The second dimension was the housing outer diameter(part 2 in Figure 33). This value has a direct relation to the magnitude and direction of flux through the MRF. In both cases, all other dimensions were also updated to maintain a constant thickness.

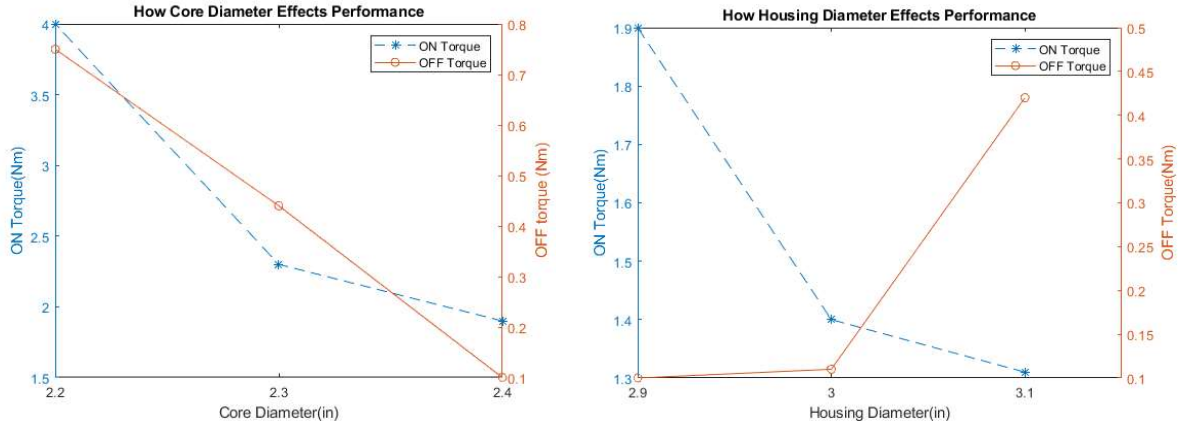

Figure 47. Parameterized dimensions and resulting simulated torque to provide design insight for future work

As expected, reducing the distance from the magnet's surface to the MRF resulted in much more ON state torque, but also increased the OFF state torque. Essentially in the OFF state, more flux is leaking

into the MRF because there is less space for it in the core. This leakage could potentially be improved by using a higher performing material like annealed Hyperco-50 for the core material as it has a higher magnetic strength and permeability than 1018 steel.

Less intuitively, as the housing diameter was increased, the ON torque decreased. This is most likely due to less flux orthogonally passing through the MRF and flowing along a more tangential path, creating less torque. The dimension only begins to effect the OFF state torque when it starts to get too large.

Other than changing geometry there are other options to increase performance in future designs. One of the most straightforward would be utilizing longer and stronger N52 grade magnets. In this design, only 1 inch long N42 were able to be sourced from a reliable supplier. With slight modifications to the internal geometry, higher ON torque should be achievable with little effect on the OFF torque. The

longer the magnet, the less distortion would be noticeable from end effects, allowing the array to produce a more uniform field.

CHAPTER 6

CONCLUSIONS

The new design was able to achieve the goal of developing a low power, controllable MRB with using permanent magnets. The device employs a unique activation mechanism, not previously studied. The most advantageous feature being able to leave the array in any activation state with no power required, only needing energy to change states. This low power requirement makes it ideal for battery operation or in cases where the device needs to be left in the ON state for long periods of time.

While the design is comparable to other MRBs when ratiometric torque, volume and power are considered, it does have noticeable drawbacks. The most apparent and expected is the slower dynamic response time when compared to coil-based brakes. Furthermore, it only produces 1.9Nm of torque which is less than traditional brakes of similar size.

In the future there are many design improvements that could be investigated now that a functional model has been developed and verified. Most notably further investigating the use of high performance magnetic materials such as Hyperco-50 and employing stronger magnets could be beneficial. Additionally, adjusting the internal brake geometry and perhaps using longer magnets to reduce the end effects and 3D losses along the length of the rotor could dramatically increase torque output, without increasing overall size.

REFERENCES

[1] J. Rainbow, "The magnetic fluid clutch," *AIEE Trans,* 1948.

[2] Y. Shiao and et al, "Optimal Design of a New Multipole Bilayer Magnetorheological Brake," *Smart Materials and Structures,* vol. 25, no. 11, 2016.

[3] T. May, "Improvement of Rotary MR-Brakes By Utilizing Serpentine Flux Path and T-Rotor," Washington State University, 2013.

[4] Y. Shiao and N. Quang-Anh, "Development of a Multi-Pole Magnetorheological Brake," *Smart Materials and Structures,* vol. 22, no. 6, 2013.

[5] D. M. Wang and et al, "A Novel High-Torque Magnetorheological Brake with a Water Cooling Method for Heat Dissipation," *Smart Materials and Structures,* vol. 22, no. 2, 20123.

[6] Rossa, Carlos and et al, "Development of a Multilayered Wide-Ranged Torque Magnetorheological Brake," *Smart Materials and Structures,* vol. 23, no. 2, 2014.

[7] LORD Co, "LORD TFD Steering Units," LORD Corporation, 2017.

[8] F. D. Goncalves, "Behavior Of Mr Fluids At High Velocities And High Shear Rates," in *Electrorheological Fluids and Magnetorheological Suspensions (ERMR 2004)*, 2005.

[9] LORD Corporation, "MRF-132DG Magneto-Rheological Fluid," LORD Corporation, 2011.

[10] J. Wu and et al, "Design and Modeling of a Multi-Pole and Dual-Gap Magnetorheological Brake with Individual Currents," *Advances in Mechanical Engineering,* vol. 8, no. 7, 2016.

[11] O. Erol and H. Gurocak, "Mr-Brake with Permanent Magnet as Passive Actuator for Haptics," in *World Haptics Conference (WHC)*, 2013.

[12] R. Rizzo and et al, "A Multi-Gap Magnetorheological Clutch with Permanent Magnet," *Smart Materials and Structures,* vol. 24, no. 7, 2015.

[13] R. Bjørk, "Comparison of Adjustable Permanent Magnetic Field Sources," *Journal of Magnetism and Magnetic Materials,* vol. 322, no. 22, pp. 3664-3671, 2010.

[14] Active Structures Laboratory , "Portable Muscular Rehabilitation Machine".

[15] F. Herlach, High Magnetic Fields, Singapore World Scientific Publishing Company, 2006.

[16] H. E. Hilton, "An adjustable linear Halbach array," *Journal of Magnetism and Magnetic Materials,* 2012.

[17] H. Gurocak, Industrial Motion Control, Wiley, 2016.

[18] R. Eisenbeis, "Using Linear Hall Effect Sensors to Measure Angle," Texas Instruments Incorporated, 2017.

[19] F. Alferink, Measuring the magnetic hysteresis, 2013.

[20] M. Akay, Magnetic Actuators and Sensors, Piscataway: IEEE Press, 2006.

[21] J. Coey, Magnetism and Magnetic Materials, Cambridge University Press, 2016.

[22] T. LeDuc, "A New Design Approach Based on Differential Evolution Algorithm for Geometric Optimization of Magnetorheological Brakes," *Smart Materials and Structures,* vol. 25, no. 12, 2016.

[23] Q. H. Nguyen and et al, "Geometric Optimal Design of a Magneto-Rheological Brake Considering Different Shapes for the Brake Envelope," *Smart Materials and Structures,* vol. 23, no. 1, 2013.

[24] C. Sarkar and H. Hirani, "Theoretical and Experimental Studies on a Magnetorheological Brake Operating under Compression plus Shear Mode," *Smart Materials and Structures,* vol. 22, no. 11, 2013.

[25] H. Sayyaadi and S. H. Zareh, "Prosthetic Knee Using of Hybrid Concept of Magnetorheological Brake with a T-Shaped Drum," in *2015 IEEE International Conference on Mechatronics and Automation (ICMA)*, 2015.

[26] P. Polcar, "Magnetorheological brake design and experimental verification," *Elektro,* 2012.

[27] C. Seung-Hyun and et al, "Torque Tracking Control of a Haptic Master Featuring Controllable," in *14th International Conference on Control, Automation and Systems (ICCAS 2014)*, Seoul, 2014.

[29] Jedryczka and et al, "FE analysis of magnetorheological brake with hybrid excitation," in *Electrodynamic and Mechatronic System (SELM), 2013 International Symposium*, 2013.

[30] D. M. Wang and et al, "A Novel High-Torque Magnetorheological Brake with a Water Cooling Method for Heat Dissipation," *Smart Materials and Structures,* vol. 22, no. 2, 2013.

APPENDIX

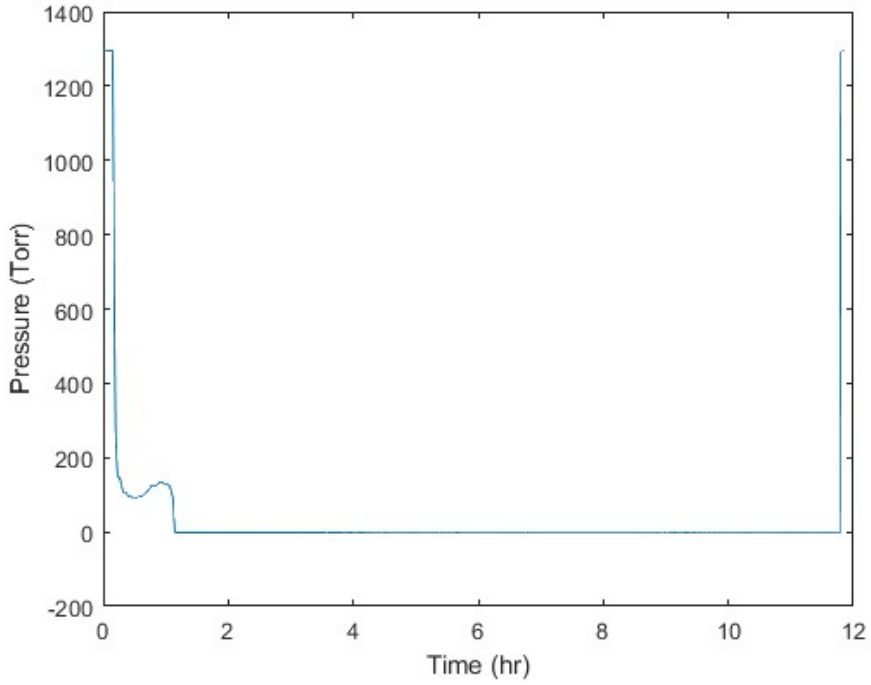

Figure 48 Carpenter Alloy 49 Vacuum Annealing pressure profile.

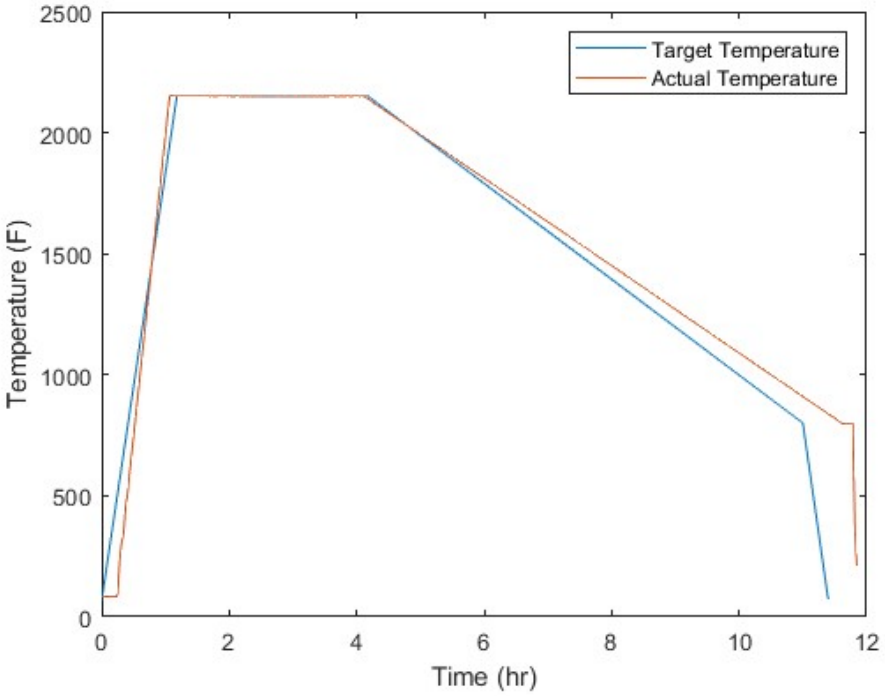

Figure 49. Carpenter Alloy 49 Vacuum Annealing temperature profile. Temperature profile was taken directly from the datasheet provided by Carpenter Tech. Co.

Figure 50. Vacuum Annealing oven used by Stack Metallurgical Co.